Impact of aliphatic acyl and aromatic thioamide substituents on the anticancer activity of Ru(II)-*p*-cymene complexes carrying acylthiourea ligands – *In vitro* and *in vivo* studies

Srividya Swaminathan,[a] Jebiti Haribabu,[a,b] Mohamed Kasim Mohamed Subarkhan,[c] Dasararaju Gayathri,[d] Nithya Balakrishnan,[a] Nattamai Bhuvanesh,[e] Cesar Echeverria[b] and Ramasamy Karvembu*[,a]

[a] *Department of Chemistry, National Institute of Technology, Tiruchirappalli 620015, Tamil Nadu, India*

[b] *Facultad de Medicina, Universidad de Atacama, Los Carreras 1579, 1532502 Copiapo, Chile*

[c] *The First Affiliated Hospital, Key Laboratory of Combined Multi-Organ Transplantation, Ministry of Public Health, School of Medicine, Zhejiang University, Hangzhou, 310003, PR China*

[d] *Centre of Advanced Study in Crystallography and Biophysics, University of Madras, Guindy Campus, Chennai 600025, India*

[e] *Department of Chemistry, Texas A & M University, College Station, Texas 77842, United States*

TABLE OF CONTENTS

Experimental section

Materials and measurements

All the chemicals and solvents were of analytical reagent grade and used without further purification. Ligands L1-L5 were synthesized according to the previously reported procedure.[1] UV-Visible spectra were recorded on a Shimadzu UV2600 instrument. FT-IR spectra of the compounds were recorded as their KBr pellets on a ThermoScientific Nicolet iS5 spectrometer. ^{1}H and ^{13}C NMR spectra were obtained by using a Bruker 500 MHz spectrometer. Mass spectra were recorded by using a Bruker Impact HD HRMS instrument. A Bruker Quest X-ray (fixed-Chi geometry) diffractometer was employed for crystal screening, unit cell determination and data collection. The goniometer was controlled using the APEX3 software suite. Olex2 was employed for the final data presentation and structure plots. All other methods related to the kinetic/biological studies are described in the following sections.[2-6]

In silico studies

Theoretical calculations of molecular physicochemical parameters, bioavailability and pharmacokinetic properties of a compound under drug discovery have gained attention over the past decade due to their fast and efficient prediction. Lipinski *et al*., were the first to present a relationship between the pharmacokinetic/physicochemical features of a compound, and its drug-likeness. The "Rule of 5", given by Christopher Lipinski in 1997, evaluates the drug-likeness based on the following features: molar mass (should be less than or equal to 500 $gmol^{-1}$), Log P (less than 5), number of H-bond acceptor and H-bond donors (less than or equal to 10 and 5, respectively).[7,8] Herein, we have carried out the *in silico* studies of the synthesized ligands and drugs that are commercially available to predict and compare their physicochemical and pharmacokinetic properties using the SwissADME web tool (**Table S4**). The %ABS is a very functional physicochemical variable that defines drug transport properties. It was calculated using the equation, $\%ABS = 109–(0.345\times TPSA)$.[8]

Molecular docking

BindingDB database was used to predict the macromolecular enzyme targets for the compounds **P1**-**P6**, and then we have proceeded with molecular docking studies. AutoDock4.2 was used for *in silico* molecular docking studies in order to investigate the binding potential of the complexes at the active site of the enzymes. Three dimensional coordinates of the enzymes (ERK1, ERK2, ERK5, JNK and p38) were downloaded from

RCSB protein data bank (PDB ids: 4QTB, 4QP7, 5BYZ, 3PTG and 1OUK, respectively). Protein preparation and complex (**P1**-**P6**) preparation were carried out using AutoDock tools. The co-crystal ligand at the active site of the enzymes was re-docked to compare its interactions with those of respective complex with the enzymes. Active site interaction images were generated using Discovery Studio.[9,10]

In vitro cytotoxicity

A549, A549cisR, and HUVEC (1×10^3 each cells/well) cells were purchased from the cell bank of the Chinese Academy of Sciences (Shanghai, China). A549 and A549cisR cells were cultured in RPMI-1640 (Gibco) supplemented with 10% fetal bovine serum (FBS, Gibco), whereas HUVEC cells were cultured in Dulbecco's modified Eagle's medium (DMEM) containing 10% FBS and 1% nonessential amino acids. All the cells were maintained at 37 °C in 5% CO_2.

Stability of the complexes

The stability of the most active complexes **P5** and **P6** was studied by ^{1}H NMR spectroscopy over a period of 24 h in DMSO(d_6)-D_2O (6:4) mixture to analyze the hydrolysis products. The complex solutions were initially prepared in DMSO-d_6, and their first spectra were recorded. Then D_2O was added, and the spectra were re-recorded over the mentioned time frame.[1]

Anti-proliferation activity

A549 cells were seeded into flat-bottomed 48-well plates (2×10^4 cells per well) and incubated at 37 °C under 5% CO_2 atmosphere for 24 h. The selected complexes and cisplatin were then added to the cells which were incubated for an additional 24 h at 37 °C. DNA synthesis was quantified at the end of the drug treatment using a Click-iTEdU Alexa Fluor 488 Assay Kit (Invitrogen) according to the manufacturer's protocol. Briefly, EdU (5-ethynyl-20-deoxyuridine) was first added to each well and the cells were incubated for 2 h at 37 °C. Then, the cells were fixed for 15 min at room temperature by adding 4% formaldehyde. Next, 0.5% Triton X-100 was added to the cells and the cells were incubated for 10 min. Subsequently, azide-labeled Alexa Fluor 488 was added to the cells, and they were incubated for 30 min in the dark. After staining the nuclei with Hoechst 33342 (Invitrogen) for 15 min, the cells were imaged using fluorescence microscopy (Olympus, IX71).[11]

Apoptosis assay

Dual AO-EB fluorescent staining was used to evaluate cell apoptosis in A549 cells upon treatment with the selected complexes and cisplatin. Briefly, cells were seeded in 24-well plates at a density of 5000 cells/well and incubated at 37 °C for 24 h. Then, the selected complexes and cisplatin were added to the cells which were incubated for 24 h. Subsequently, the staining solution (10 mL) containing AO (100 mg/mL) and EB (100 mg/mL) was added to each well (500 mL). The cells were immediately visualized using a fluorescence microscope (Olympus, BX-60, Japan), and the percentage of dead cells was quantified in at least three random microscopic fields.[11]

Flow cytometric studies

A549 cells were seeded into 6-well plates, incubated at 37 °C, and allowed to attach for 24 h. Then, fresh medium containing 1 mM of complex or cisplatin was added, and again the cells were incubated for 24 h. The untreated cells were included as control. After drug treatment, the cells were centrifuged at 1000 RPM for 5 min, washed with cold PBS and fixed with 75% ethanol at 4 °C overnight. The cells were then collected and washed twice with PBS. After that, the cells were stained with a solution containing propidium iodide (PI) (50 mg/mL) and incubated in the dark for 30 min. Cell cycle distribution was then analyzed with a BD FACSCanto™ II flow cytometer. The cell apoptotic rate was determined by flow cytometry analysis with a fluorescein isothiocyanate (FITC) Annexin V apoptosis detection kit (Multi Sciences, China). A549 cells were collected by trypsinization, washed twice, and re-suspended in 500 mL of 1N binding buffer with 5 mL of FITC Annexin V and 10 mL of PI. After incubation for 15 min, the samples were subjected to analysis by flow cytometry. The results were analyzed with the BD FACS Calibur™ system.[11]

Systemic in vivo toxicity

All the animal studies were conducted following the National Institute Guide for the care and use of laboratory animals. The experimental protocols were approved by the ethics committee of the First Affiliated Hospital, Zhejiang University School of Medicine. Healthy Institute of Cancer research (ICR) mice (4-5 weeks old) were randomized into groups (n = 8, four females and four males in each group) and intraperitoneally injected with different doses of **P6** solution in DMSO (50 mL) every other day for five times. Saline, DMSO, and cisplatin solution (Hospira Australia Pty Ltd.) were used as controls. Cisplatin was administered at doses of 2 and 4 mg/kg. **P6** was administered at doses of 2, 4, 8 and 16 mg/kg. The body weight changes of mice were monitored. After receiving two saline injections, DMSO,

cisplatin or **P6**, two mice in each group were randomly selected and sacrificed by CO_2 inhalation. The major organs such as kidney, liver, lung and spleen were collected and fixed with 4% formaldehyde. Then, the tissues were embedded in paraffin and sectioned into 5 mm thick slices. These slices were stained with hematoxylin and eosin (H & E, Sigma).[11]

Results and discussion

Characterization

The UV-Visible data of the compounds were collected in methanol. Mostly, ligands L1, L3 and L5 displayed similar spectra while L2, L4 and L6 showed alike spectra. They could only be differentiated through $\sigma \rightarrow \sigma^*$ transition which falls below the wavelength observable on a laboratory spectrophotometer. However, the former set could be differentiated from the latter one in terms of N-terminal substituent. A similar pattern was observed in the case of the complexes as well. The $n \rightarrow \pi^*$ and $\pi \rightarrow \pi^*$ transitions were observed at 313-295 and 275-216 nm, respectively in the spectra of the complexes. These transitions appeared at longer wavelengths in the spectra of the complexes compared to those of the ligands. Additionally, a $d \rightarrow d$ transition (413-436 nm) was observed for the complexes (**Figures S1-S2**).[1,12,13]

The FT-IR spectra of the ligands and complexes were quite complex as the aliphatic C–H stretching frequencies coincided with the characteristic stretching frequencies of thiourea and thioamide N–H. However, the spectra of the complexes displayed a typical shift in the ν(C=S) stretching to lower wave number upon coordination of the acylthiourea ligands to Ru ion *via* S atom. Other stretching frequencies showed insignificant changes, which can be further attributed to monodentate coordination of the acylthiourea ligands (**Figures S3-S14**).[1,12,13]

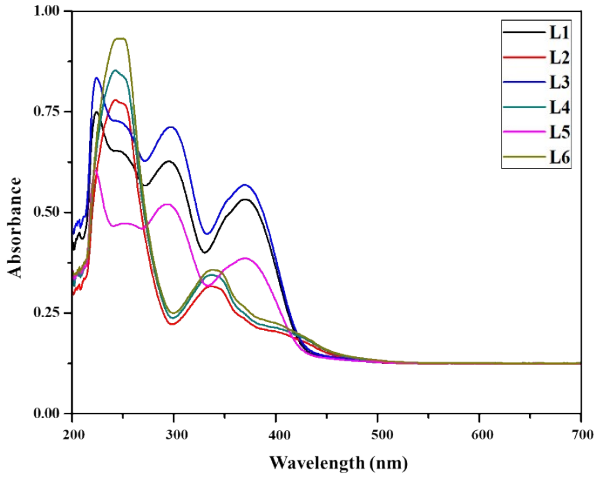

Figure S1. UV-Visible spectra of L1-L6.

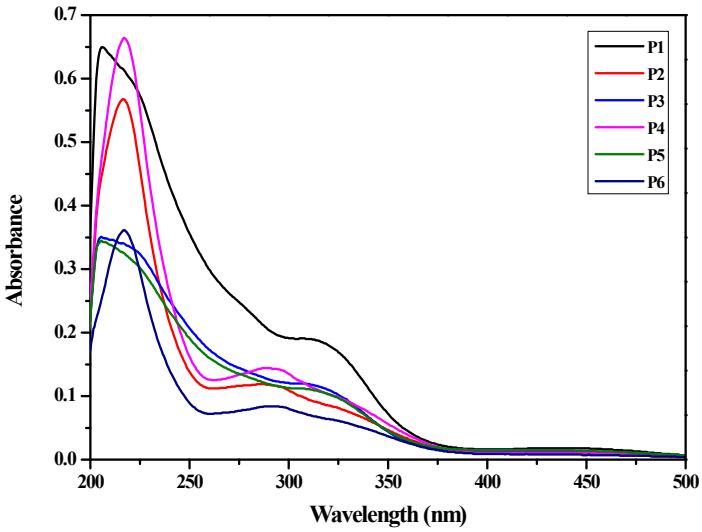

Figure S2. UV-Visible spectra of **P1-P6**.

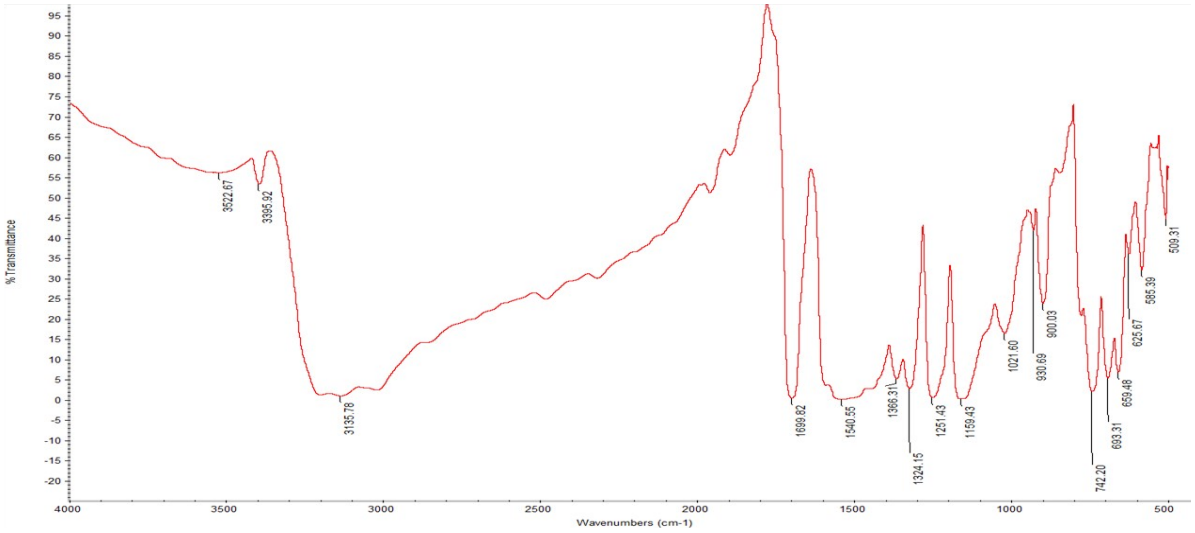

Figure S3. FT-IR spectrum of L1.

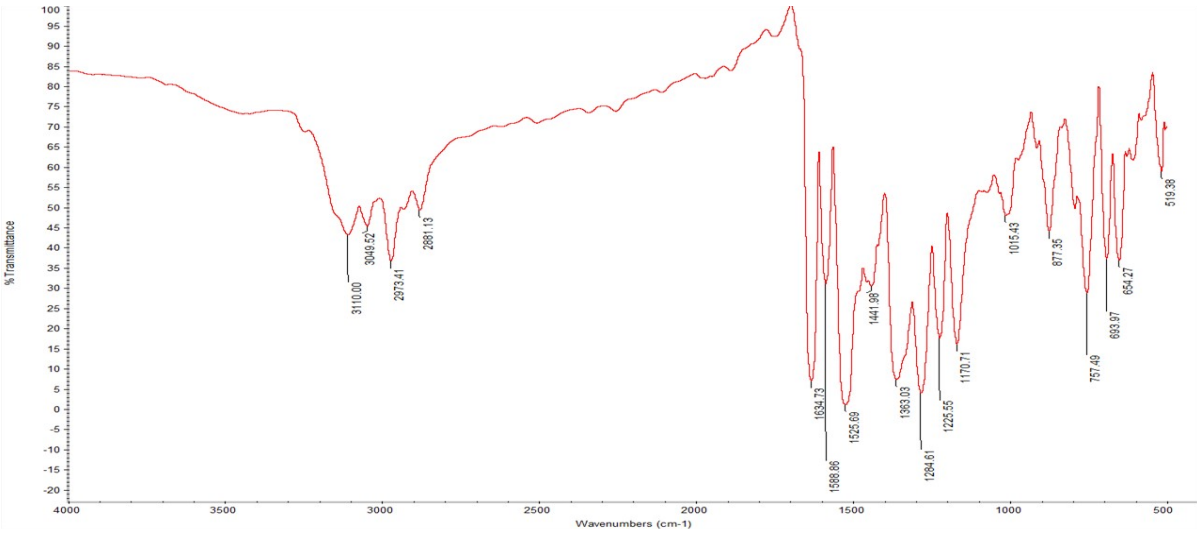

Figure S4. FT-IR spectrum of **P1**.

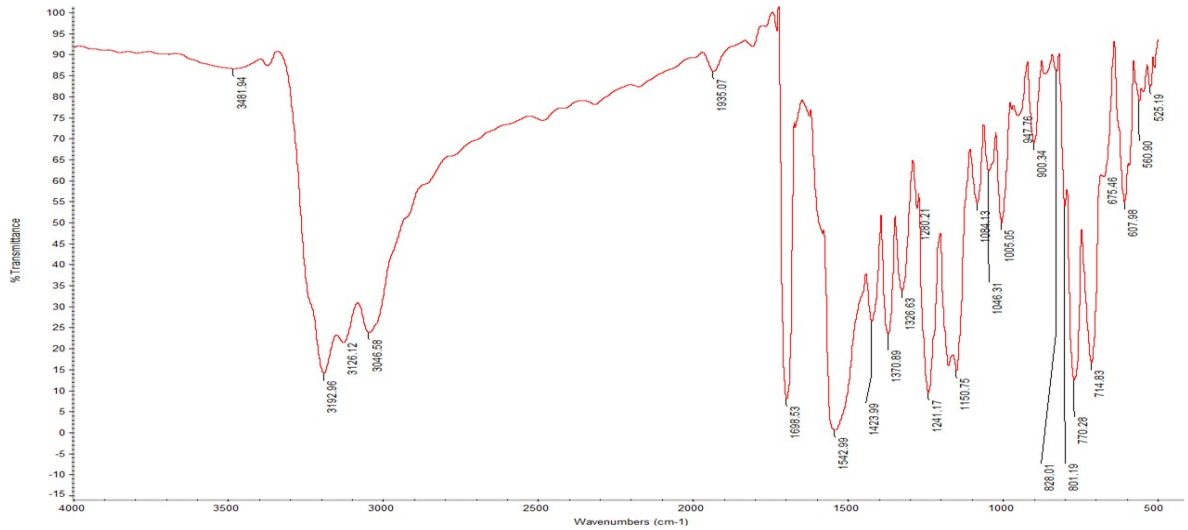

Figure S5. FT-IR spectrum of L2.

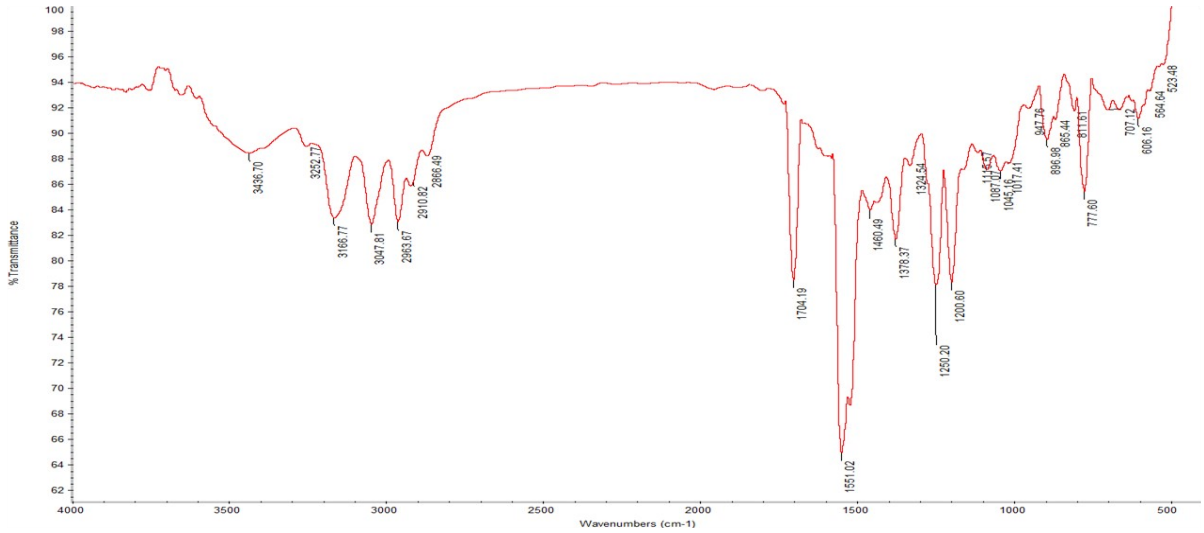

Figure S6. FT-IR spectrum of **P2**.

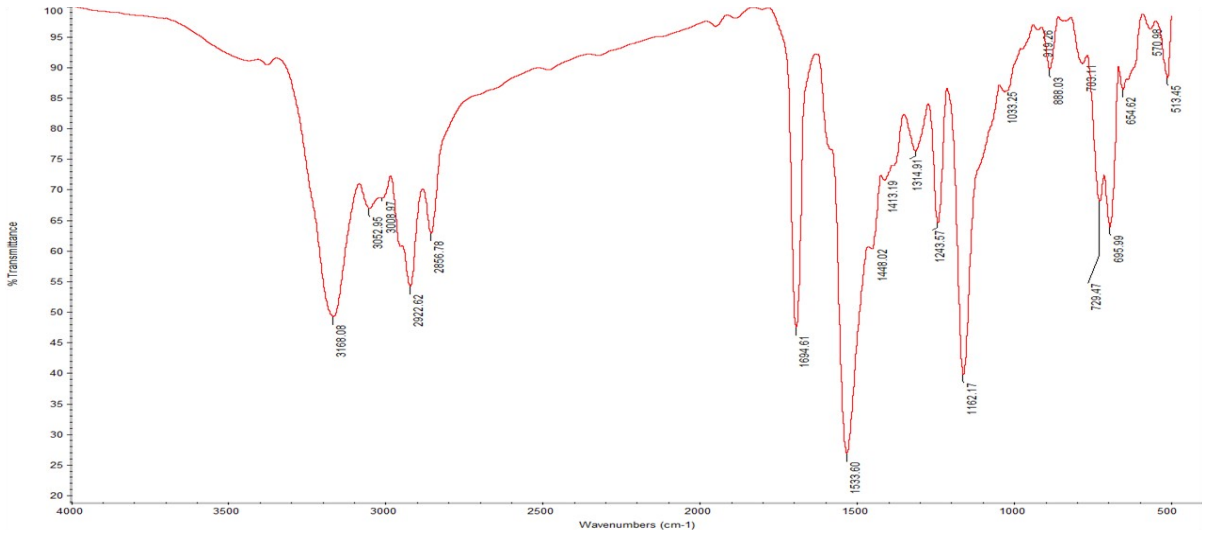

Figure S7. FT-IR spectrum of L3.

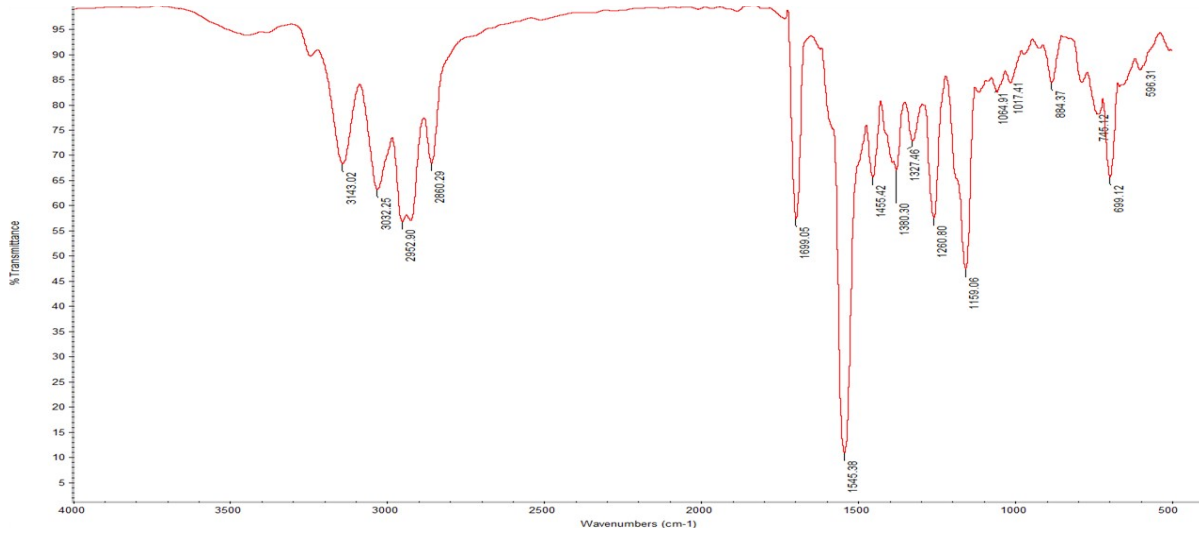

Figure S8. FT-IR spectrum of **P3**.

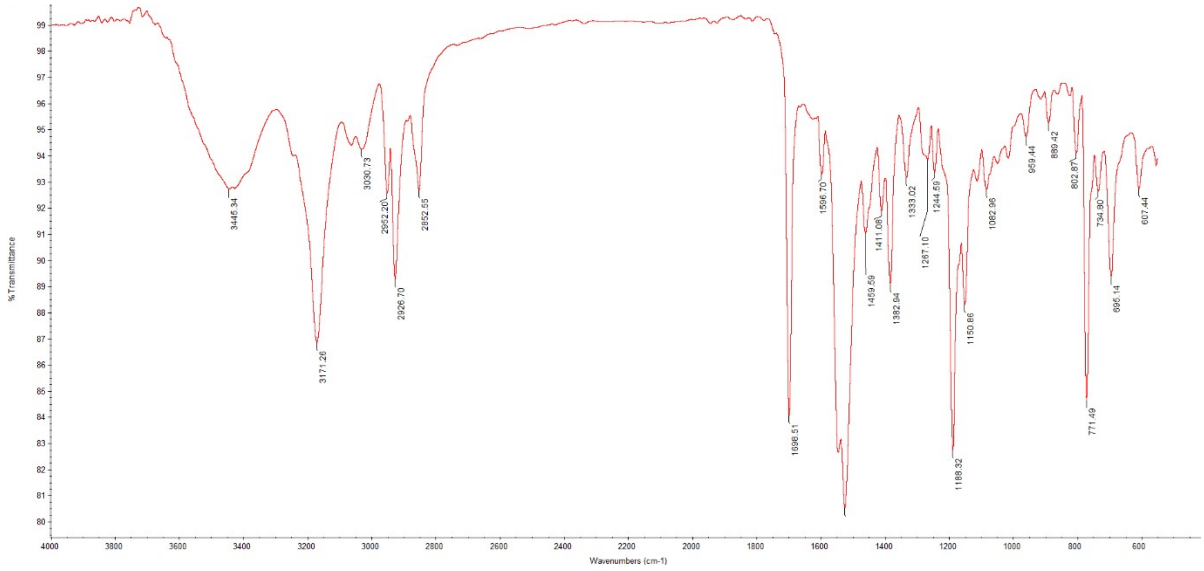

Figure S9. FT-IR spectrum of L4.

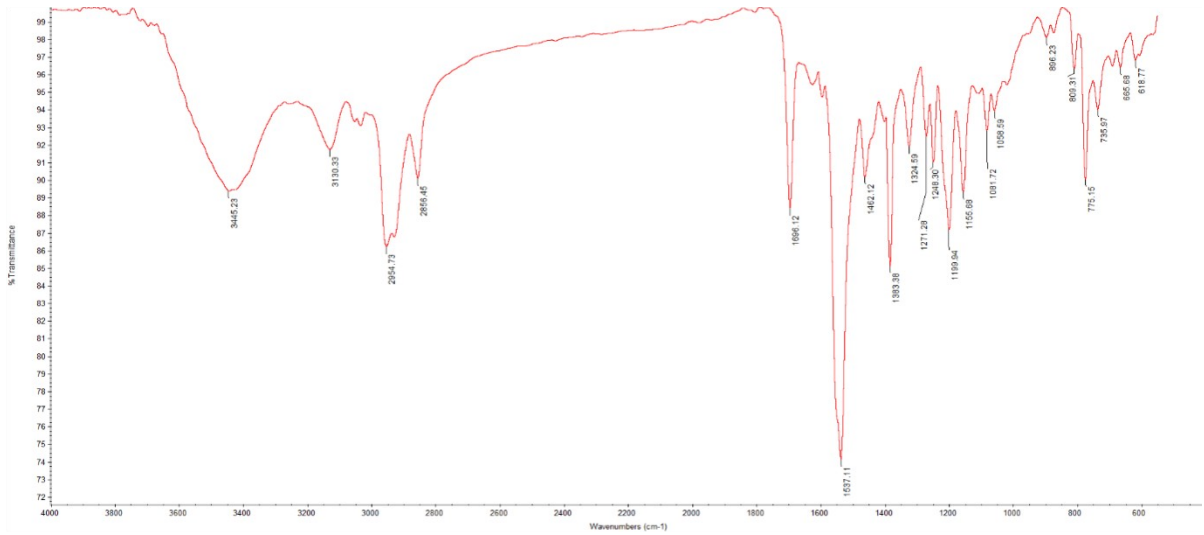

Figure S10. FT-IR spectrum of **P4**.

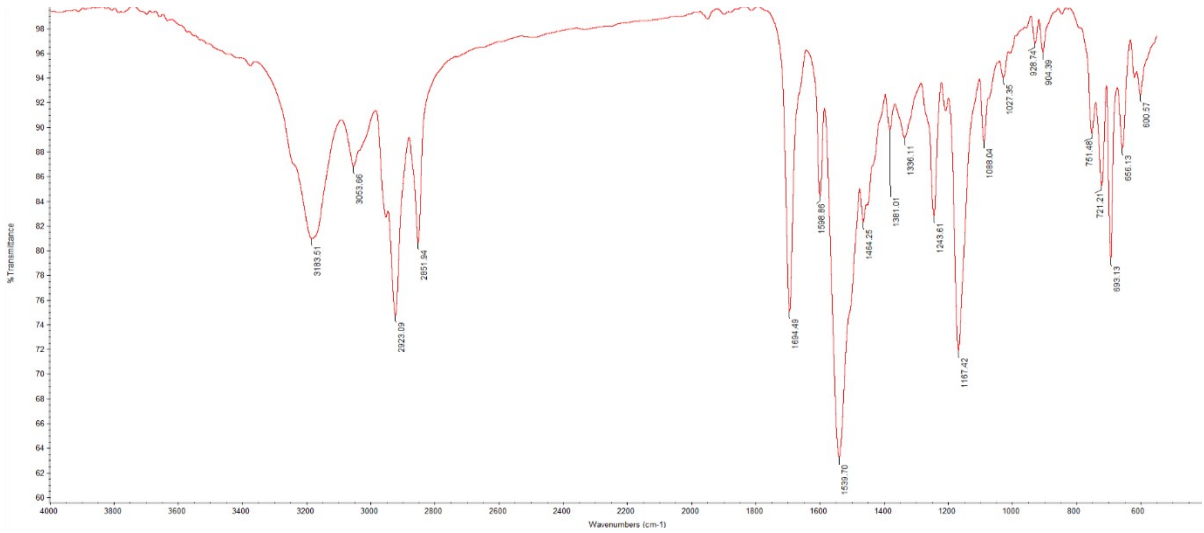

Figure S11. FT-IR spectrum of L5.

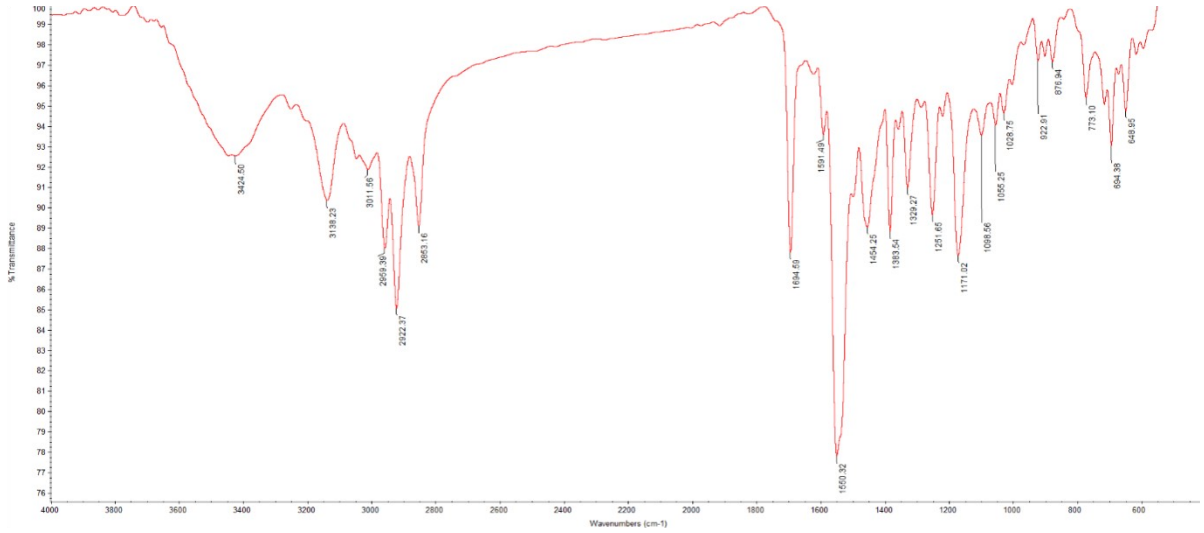

Figure S12. FT-IR spectrum of **P5**.

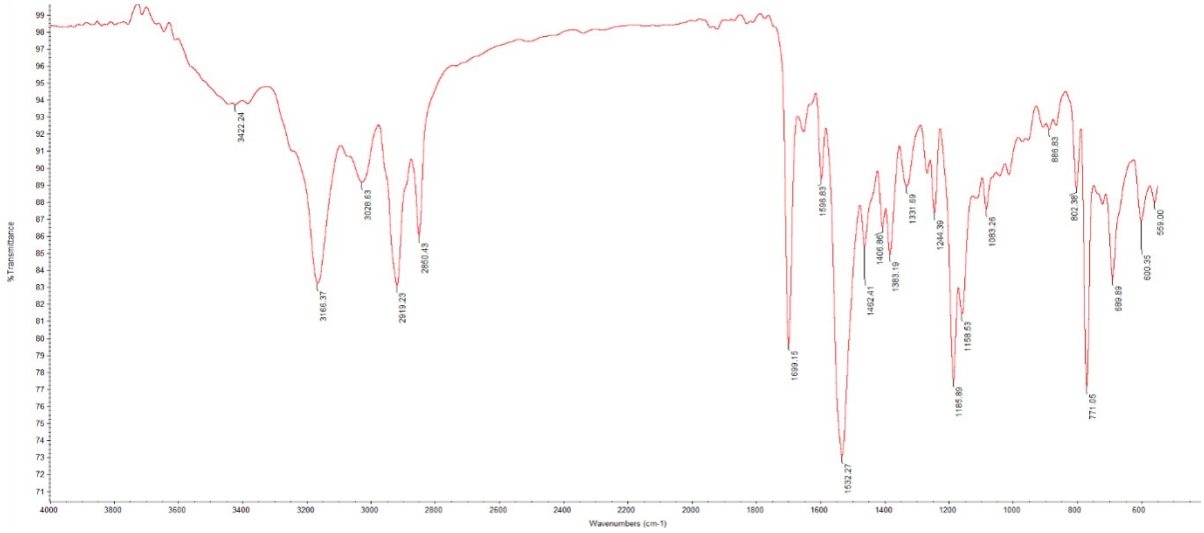

Figure S13. FT-IR spectrum of L6.

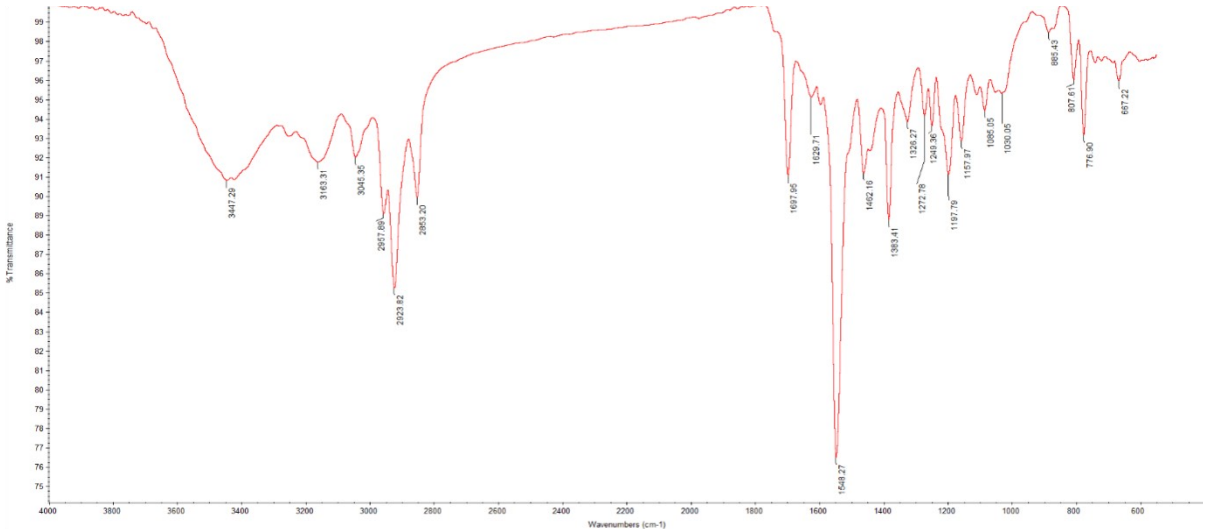

Figure S14. FT-IR spectrum of **P6**.

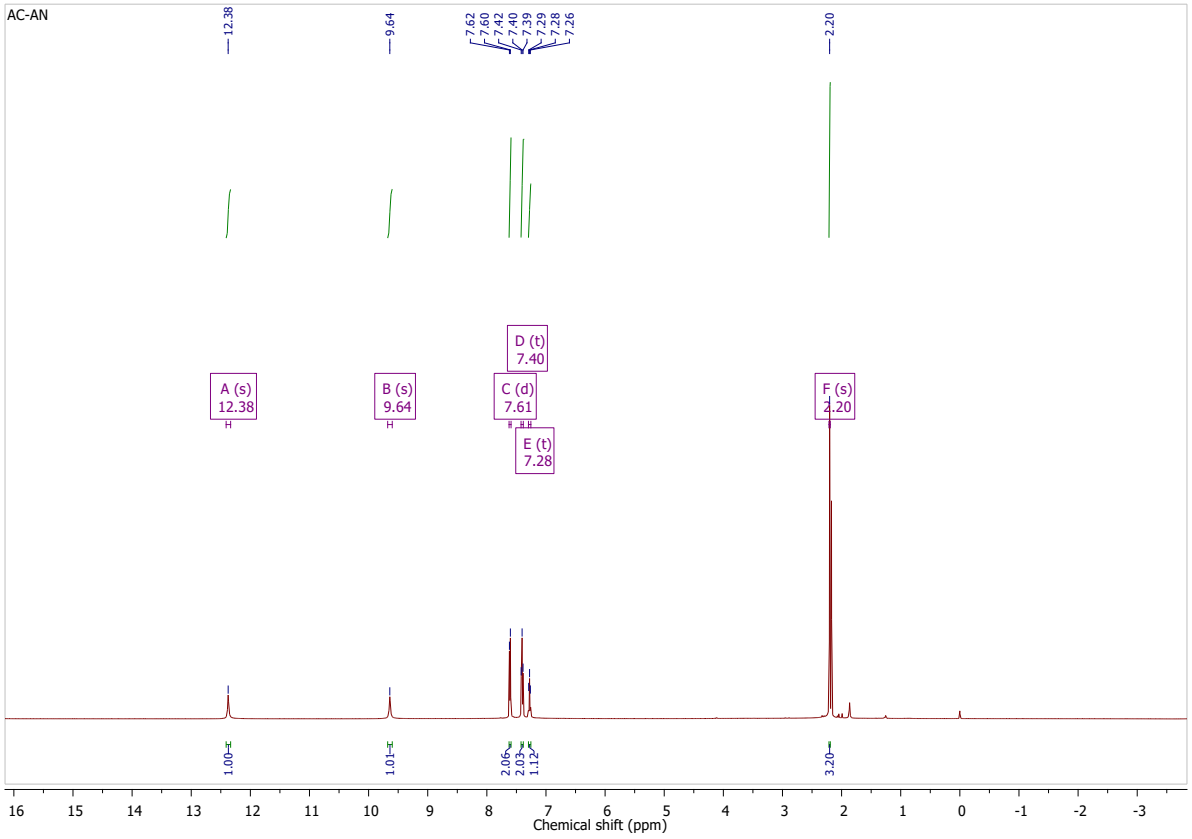

Figure S15. ^{1}H NMR spectrum (500 MHz, $CDCl_3$) of L1.

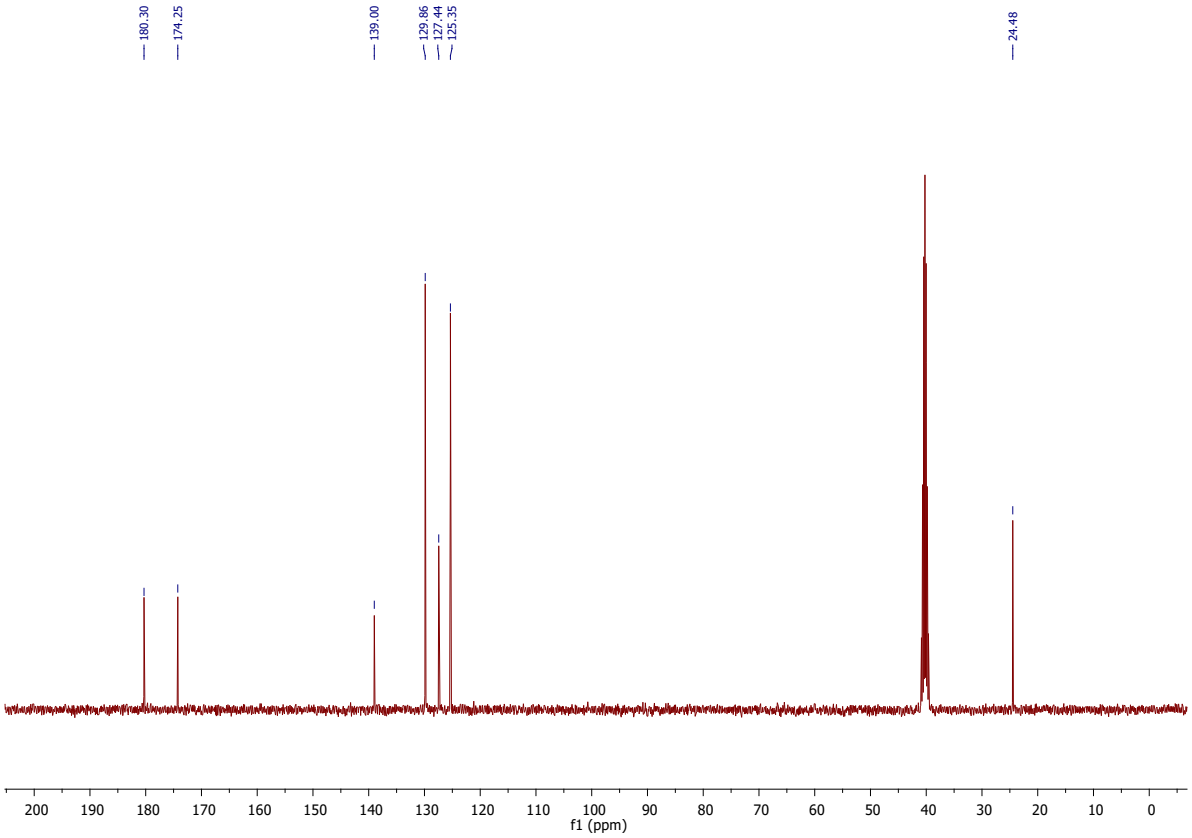

Figure S16. $^{13}C\{^{1}H\}$ NMR spectrum (100 MHz, DMSO-d_6) of L1.

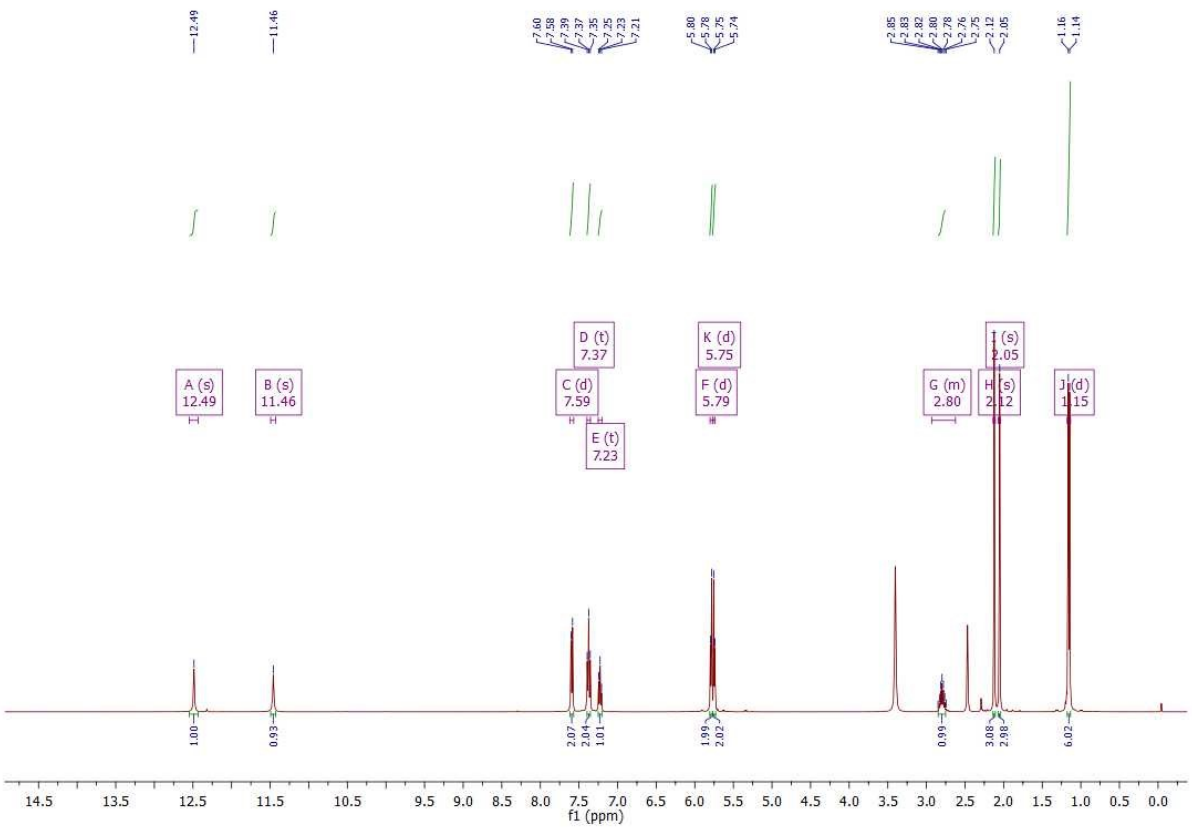

Figure S17. ^{1}H NMR spectrum (400 MHz, DMSO-d_6) of **P1**.

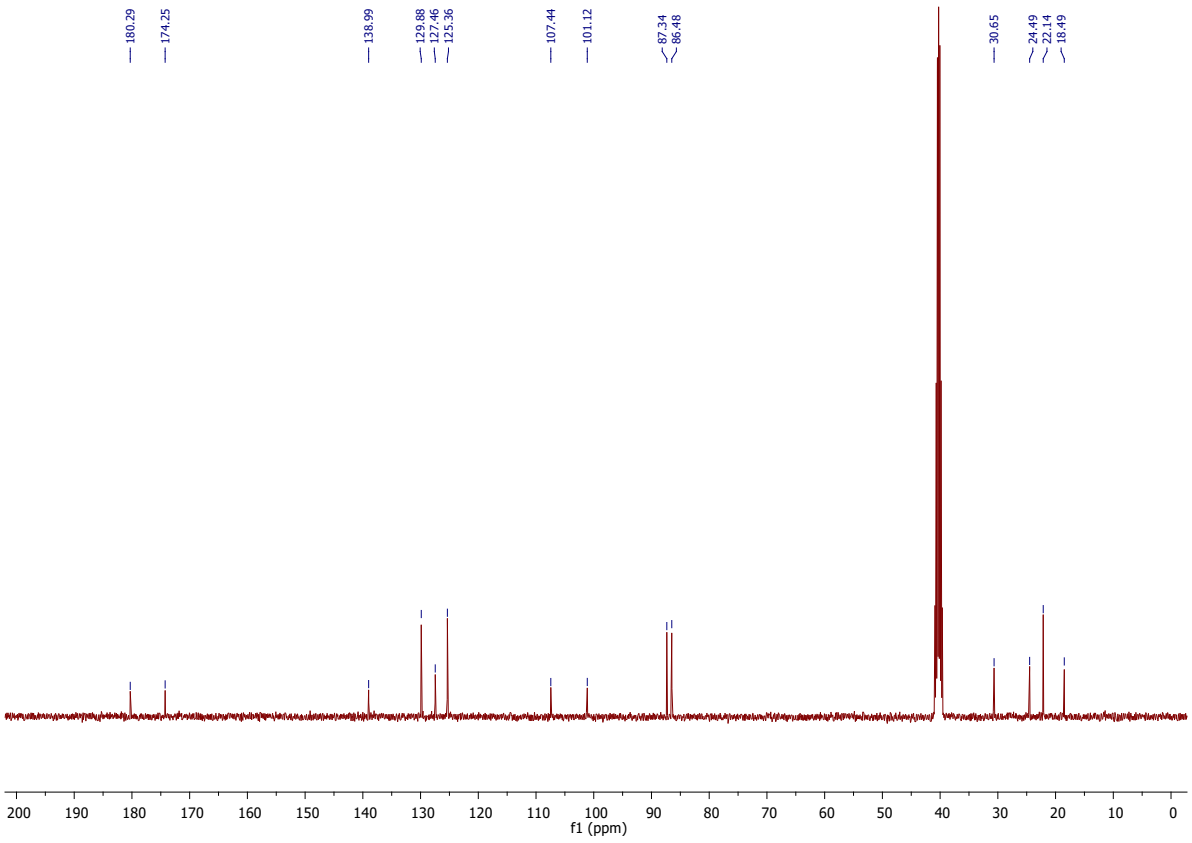

Figure S18. ^{13}C{^{1}H} NMR spectrum (100 MHz, DMSO-d_6) of **P1**.

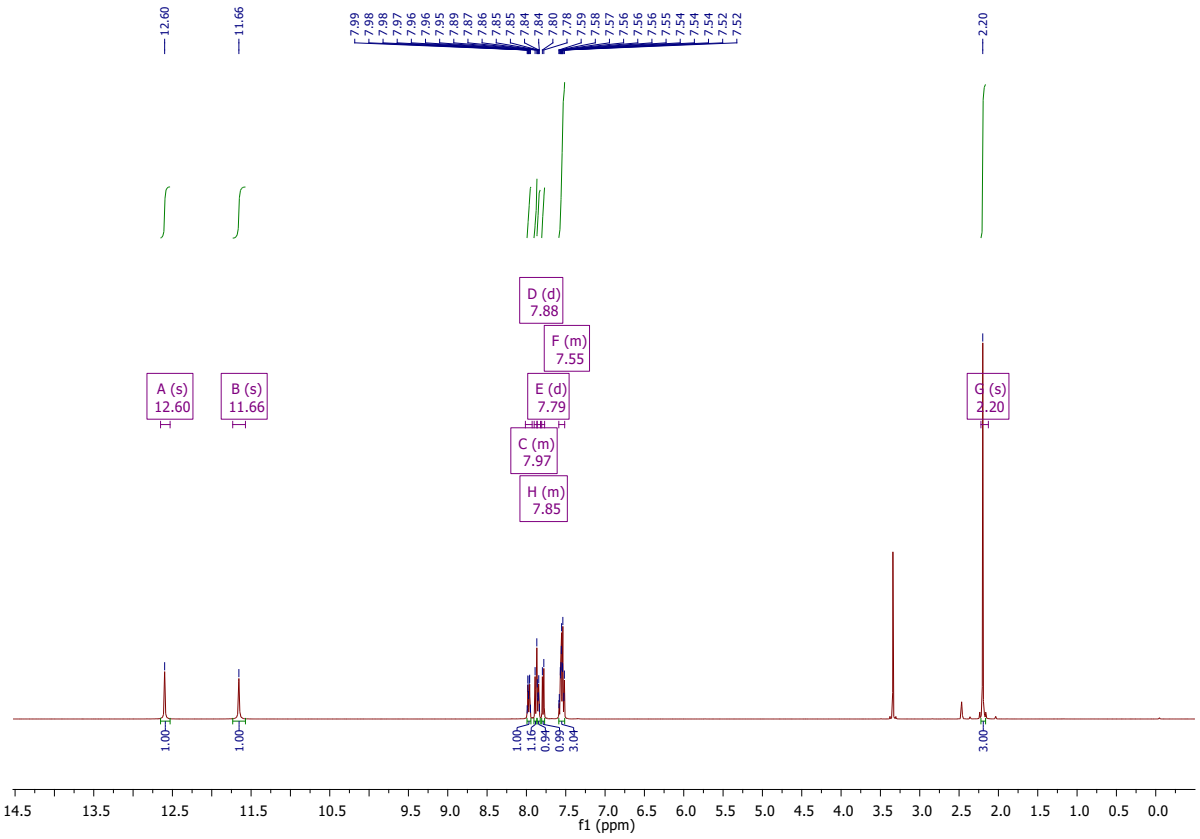

Figure S19. ^{1}H NMR spectrum (400 MHz, DMSO-d_6) of L2.

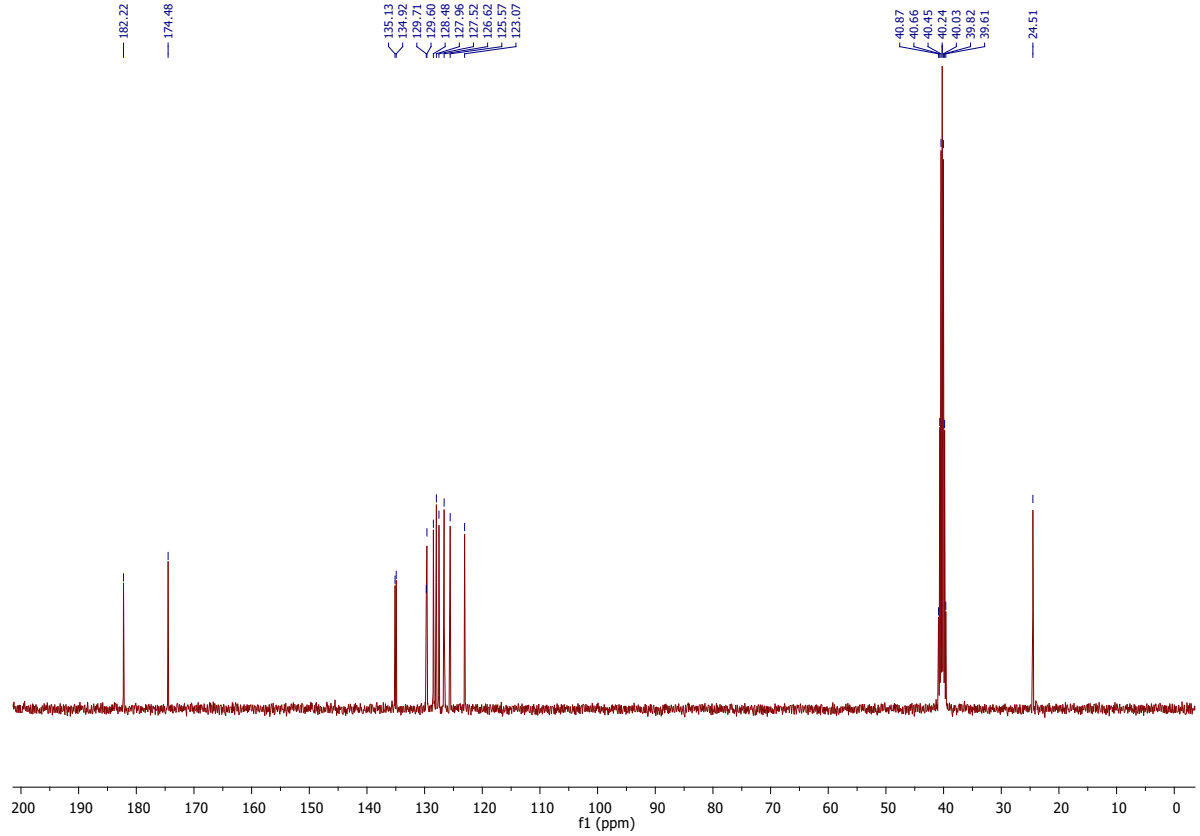

Figure S20. ^{13}C{^{1}H} NMR spectrum (100 MHz, DMSO-d_6) of L2.

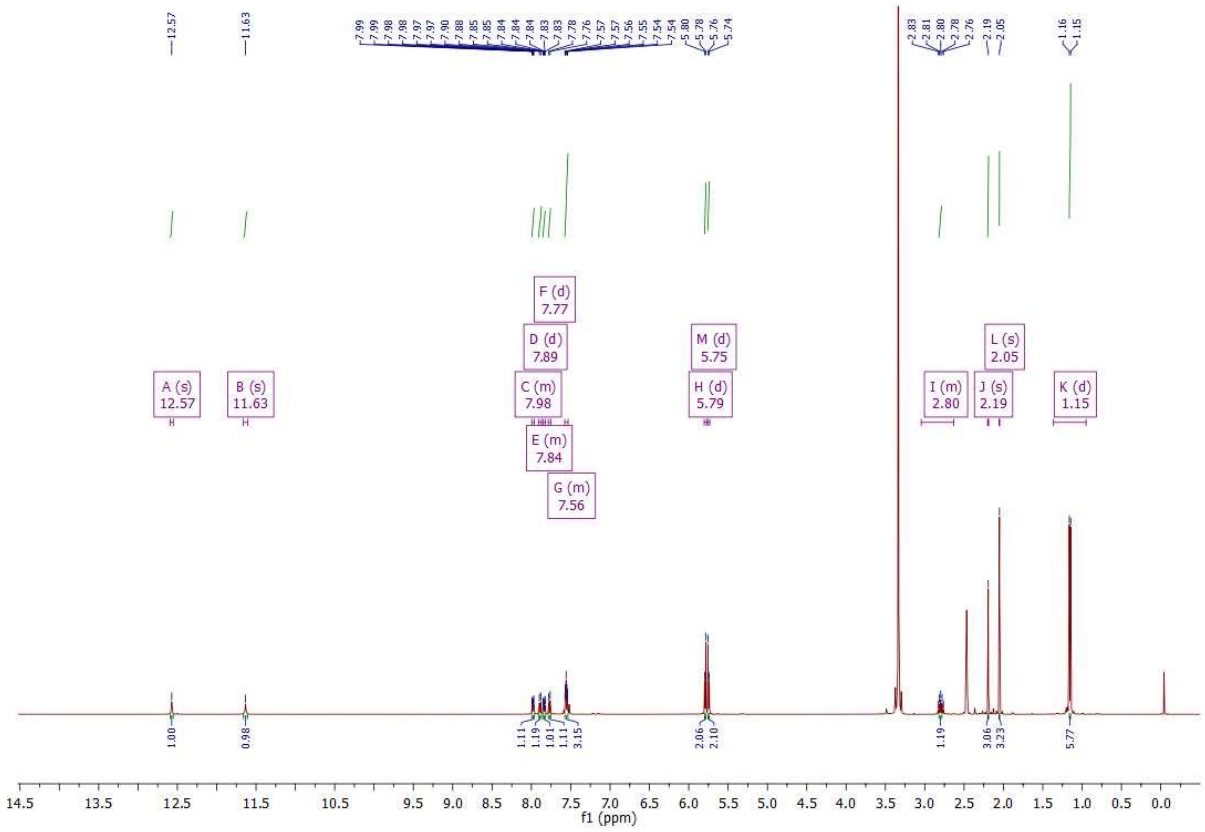

Figure S21. ^{1}H NMR spectrum (400 MHz, DMSO-d_6) of **P2**.

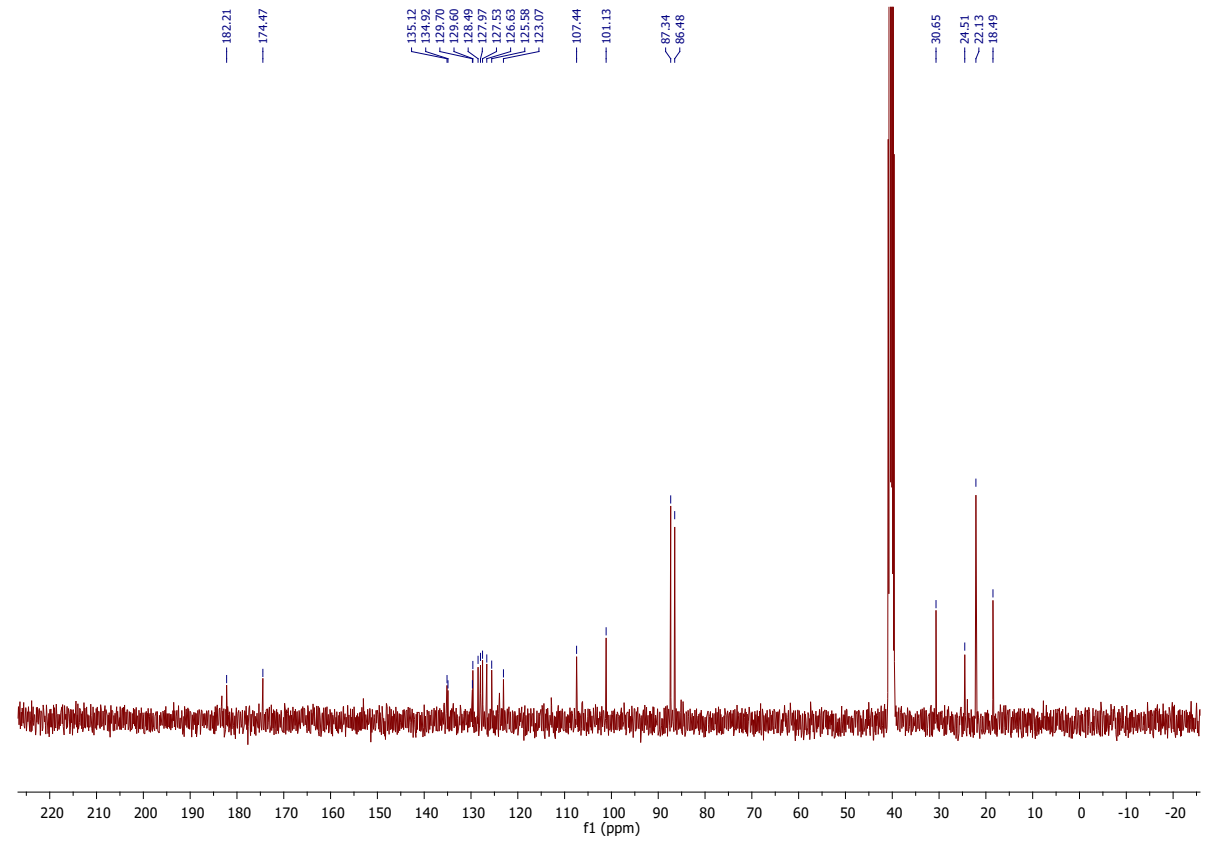

Figure S22. ^{13}C{^{1}H} NMR spectrum (100 MHz, DMSO-d_6) of **P2**.

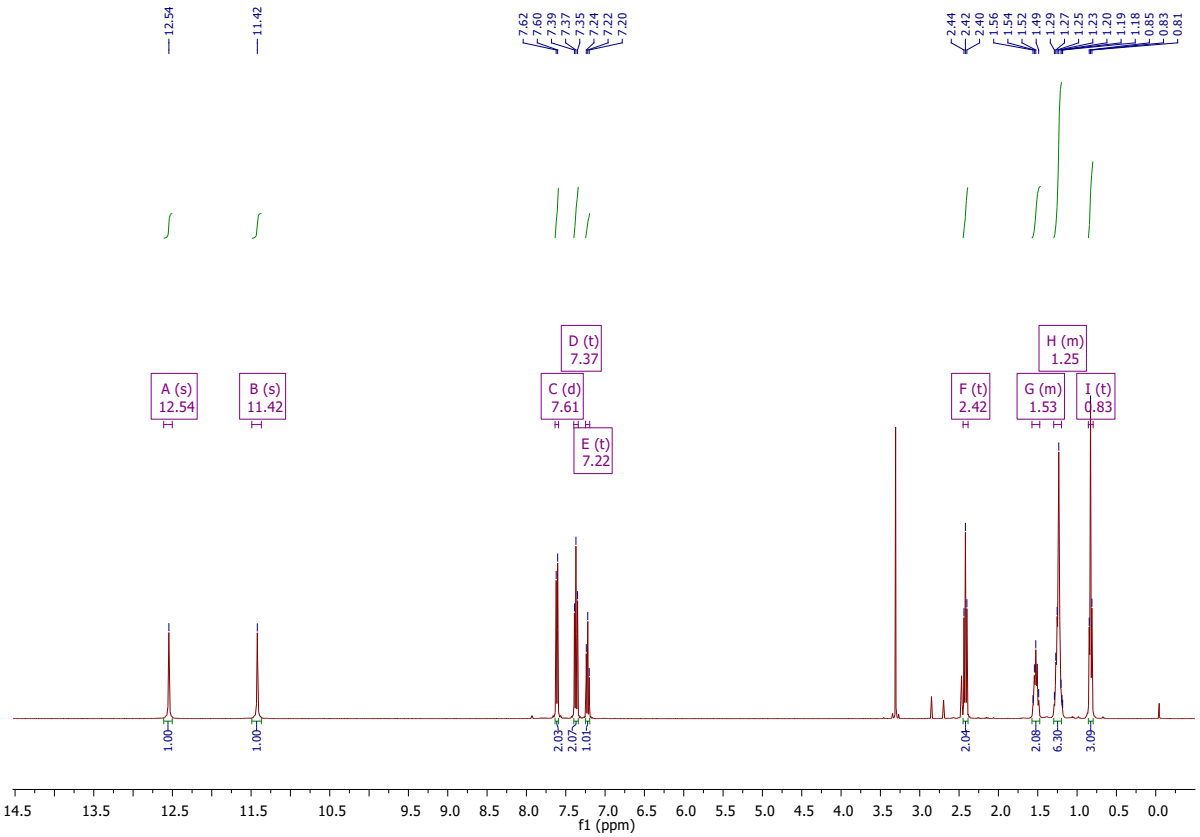

Figure S23. ^{1}H NMR spectrum (400 MHz, DMSO-d_6) of L3.

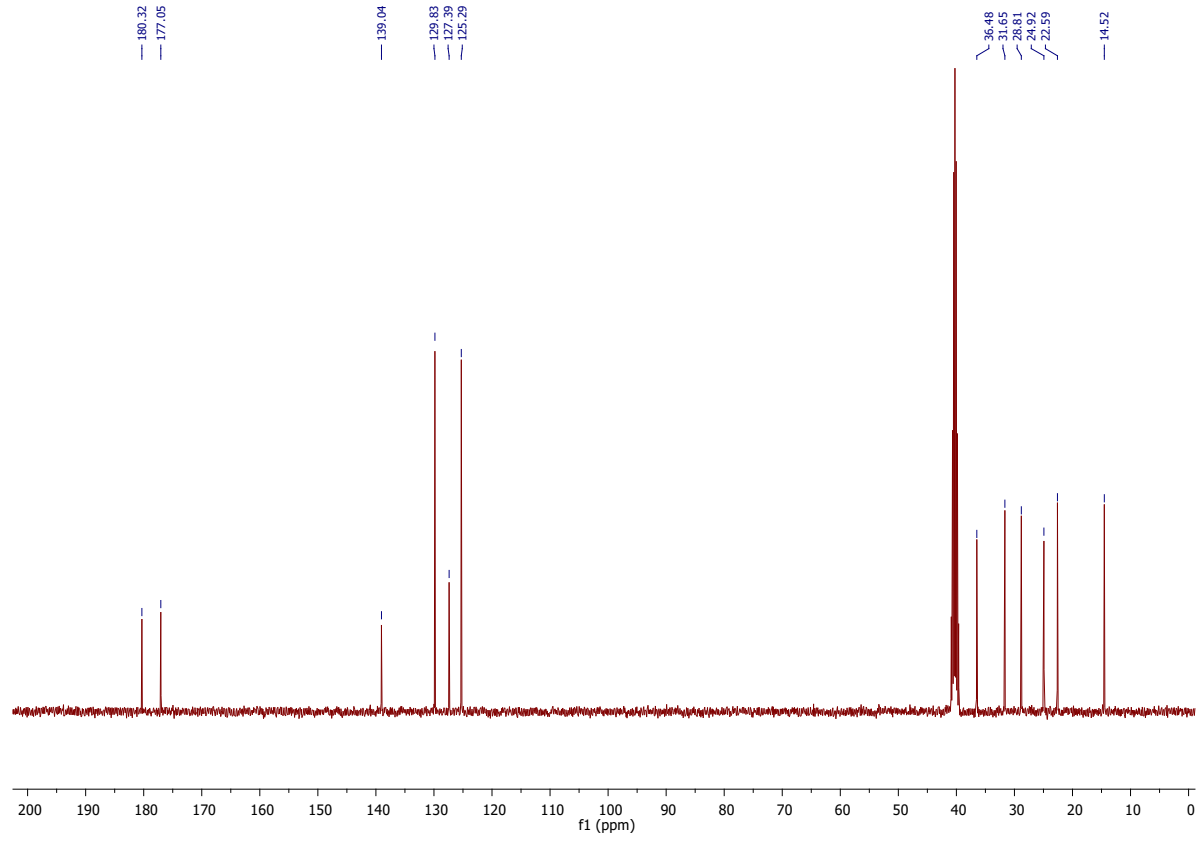

Figure S24. ^{13}C{^{1}H} NMR spectrum (100 MHz, DMSO-d_6) of L3.

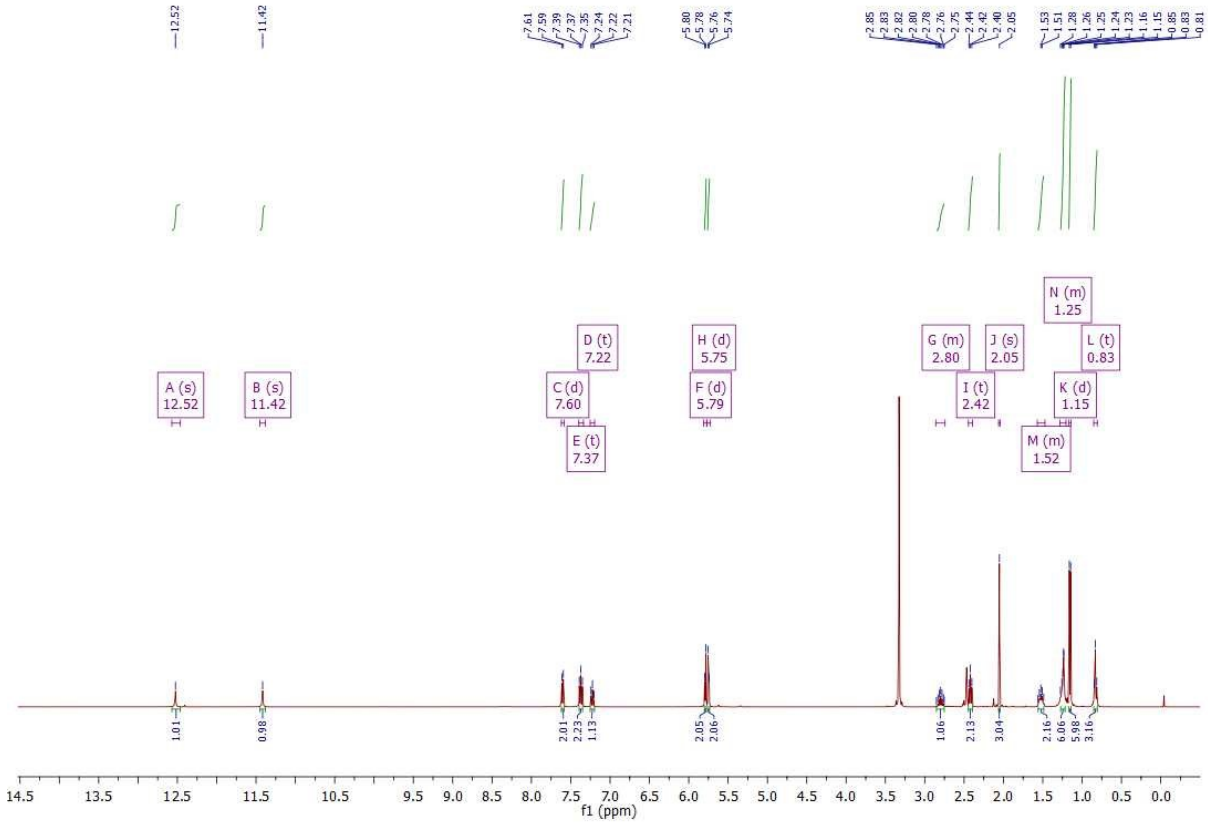

Figure S25. ^{1}H NMR spectrum (400 MHz, DMSO-d_6) of **P3**.

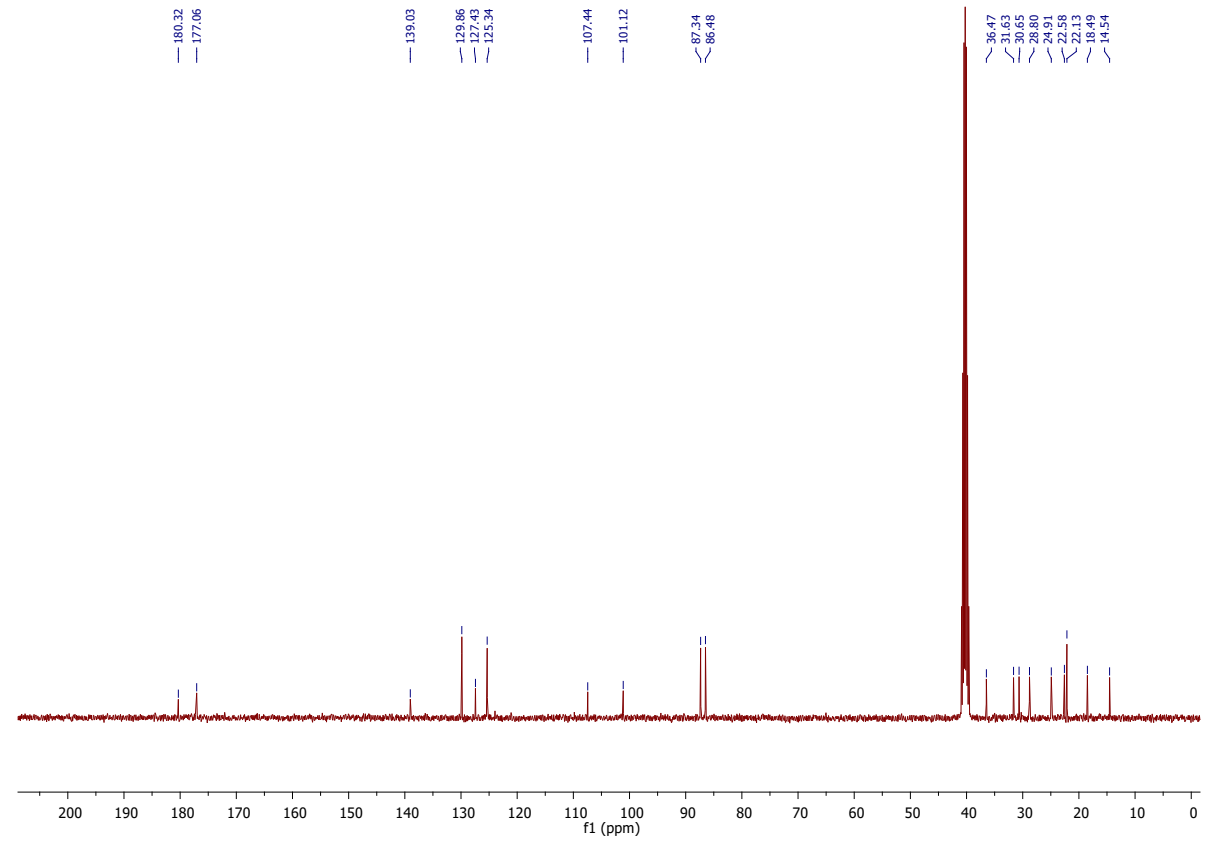

Figure S26. ^{13}C{^{1}H} NMR spectrum (100 MHz, DMSO-d_6) of **P3**.

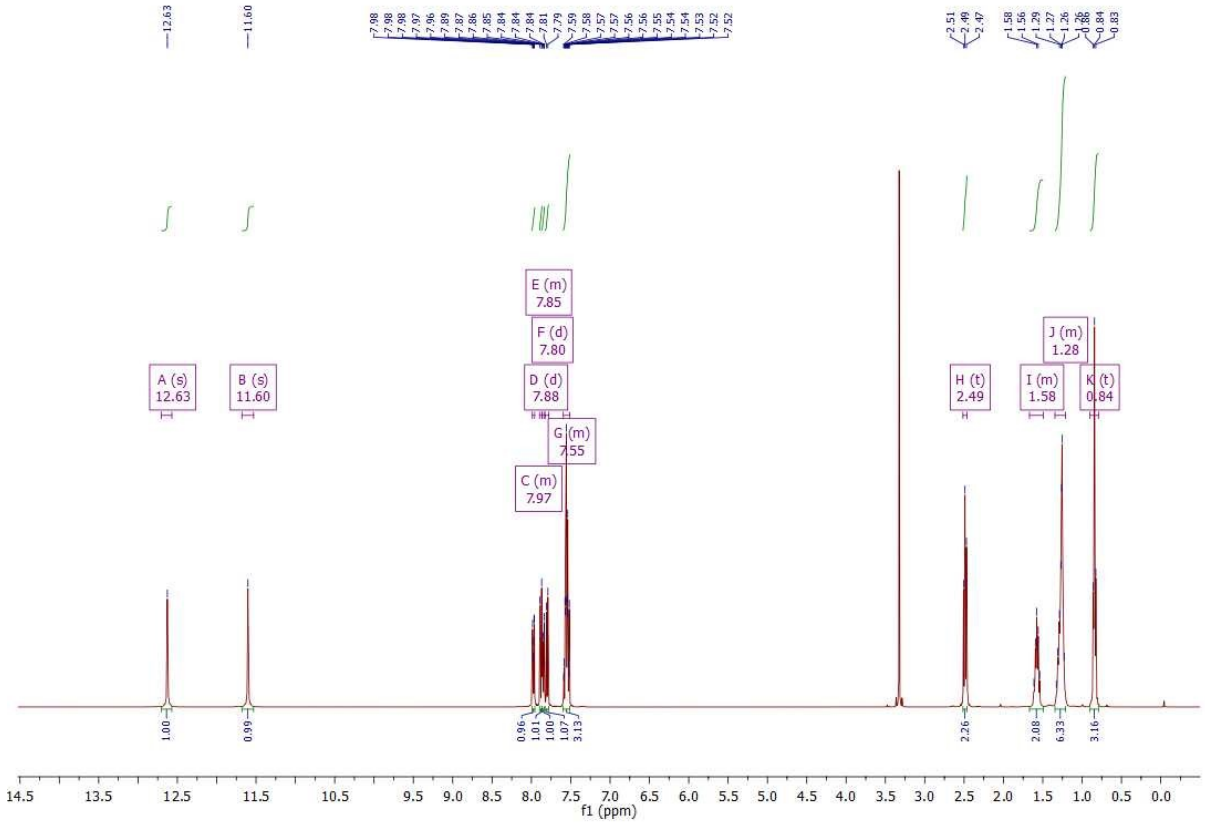

Figure S27. ^{1}H NMR spectrum (400 MHz, DMSO-d_6) of L4.

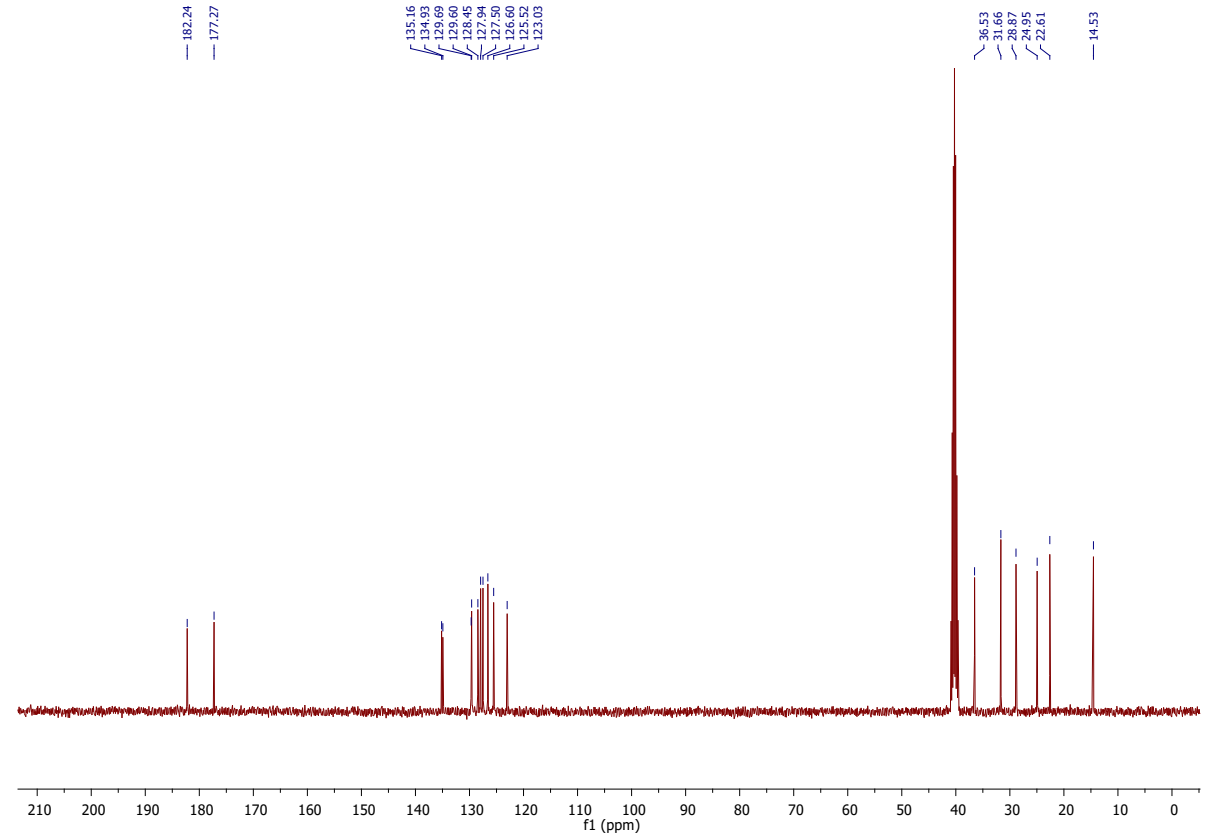

Figure S28. ^{13}C{^{1}H} NMR spectrum (100 MHz, DMSO-d_6) of L4.

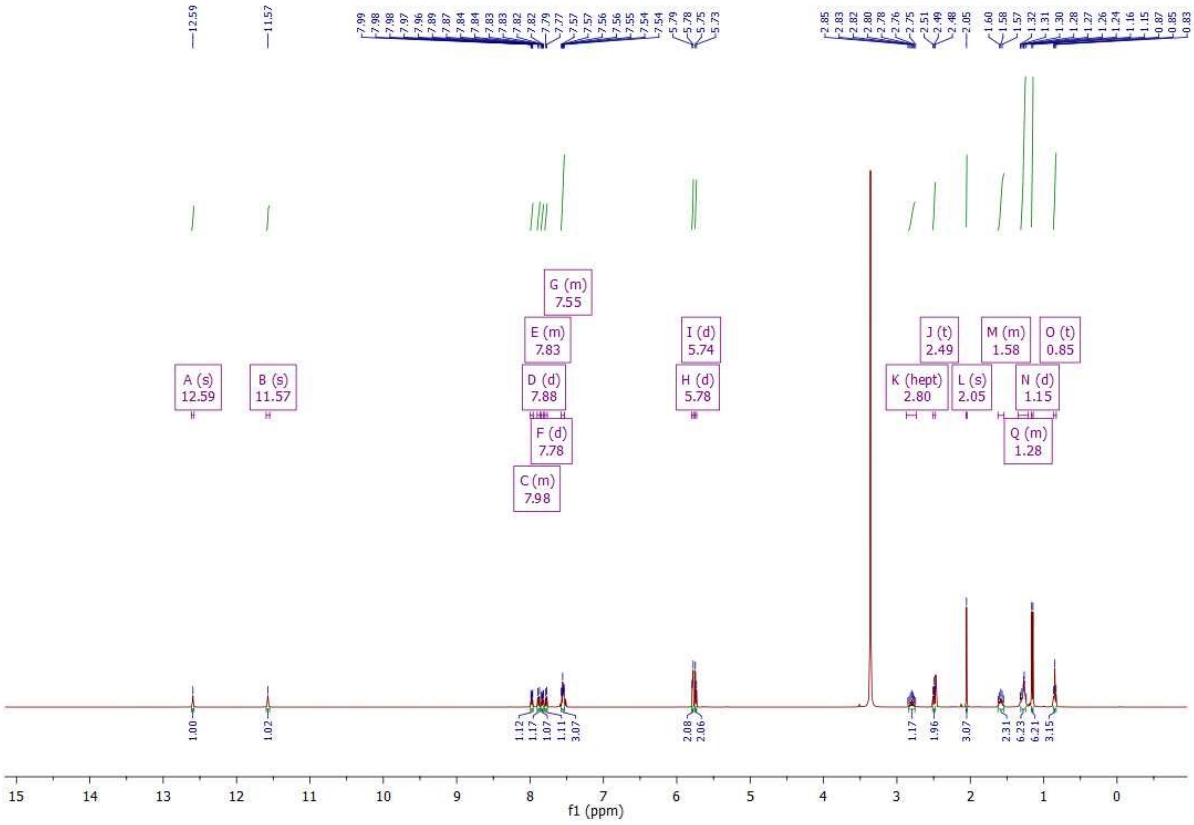

Figure S29. ^{1}H NMR spectrum (400 MHz, DMSO-d_6) of **P4**.

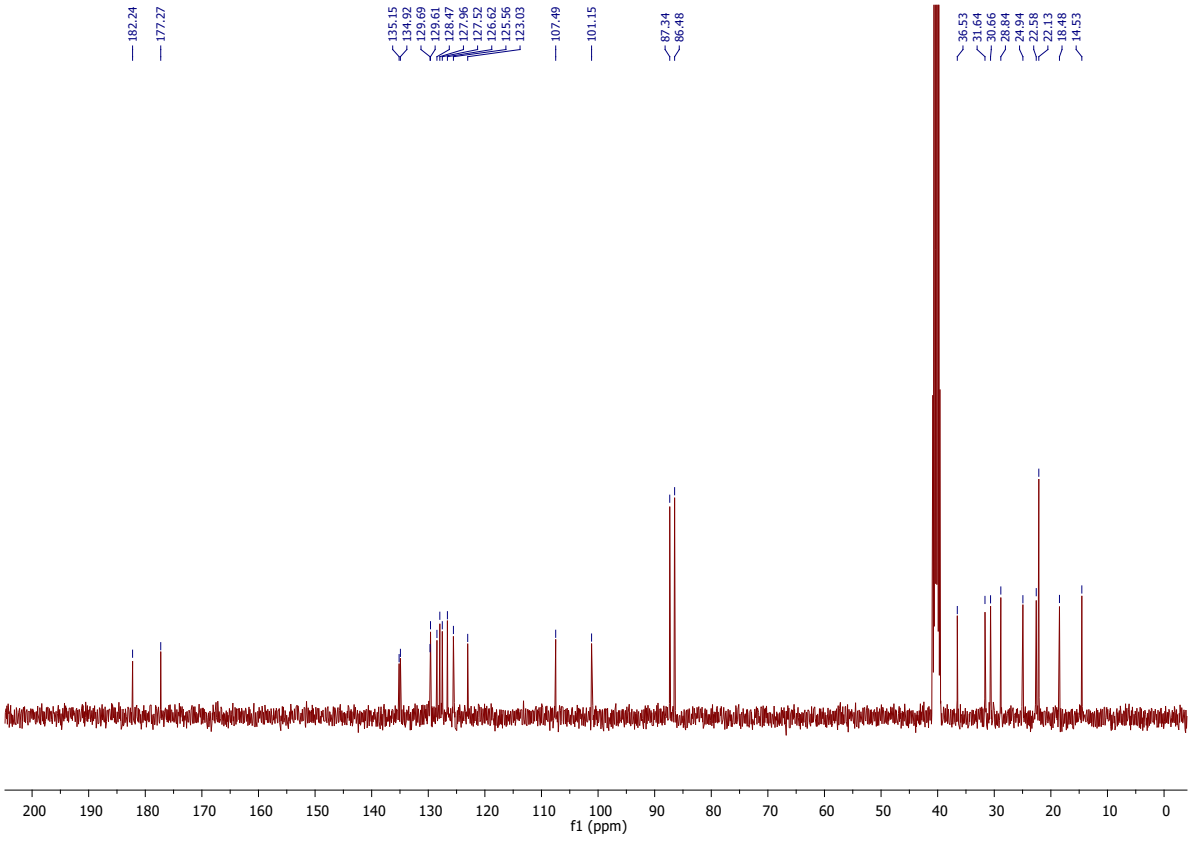

Figure S30. ^{13}C{^{1}H} NMR spectrum (100 MHz, DMSO-d_6) of **P4**.

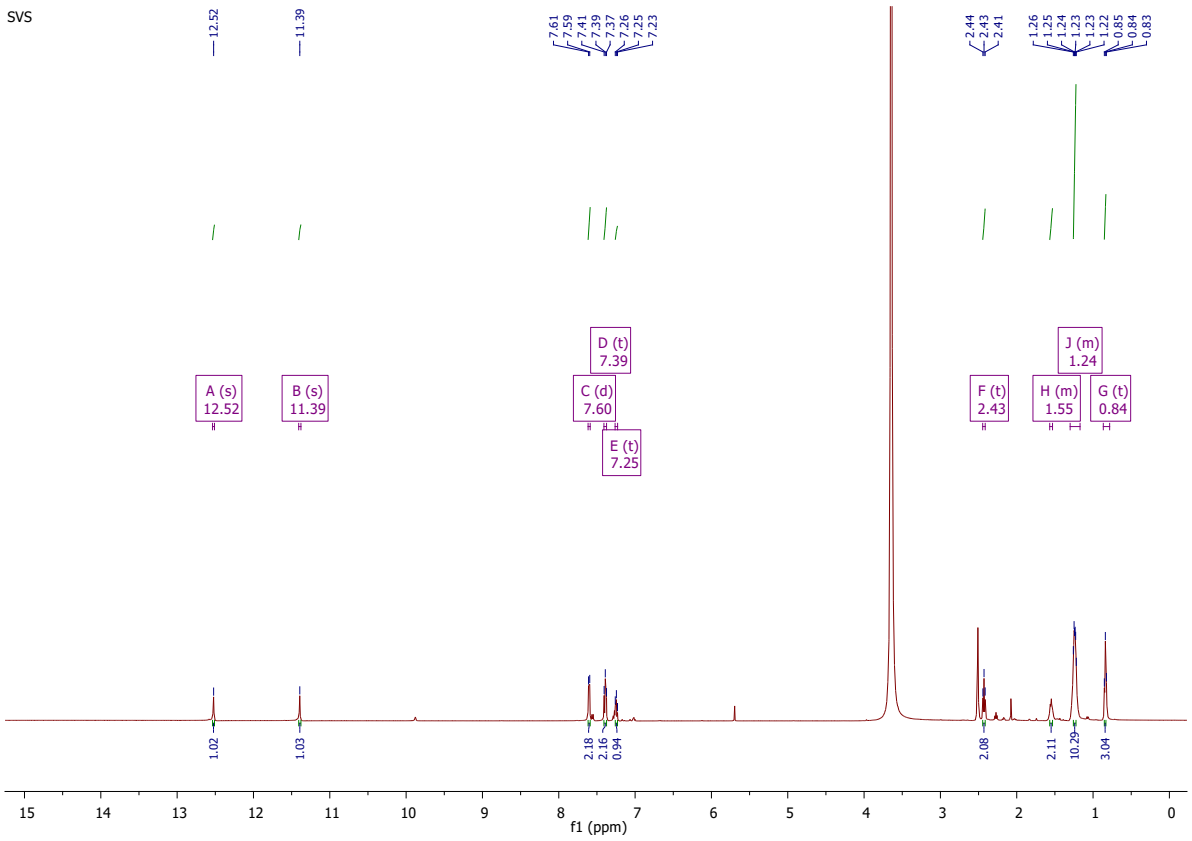

Figure S31. ^{1}H NMR spectrum (400 MHz, DMSO-d_6) of L5.

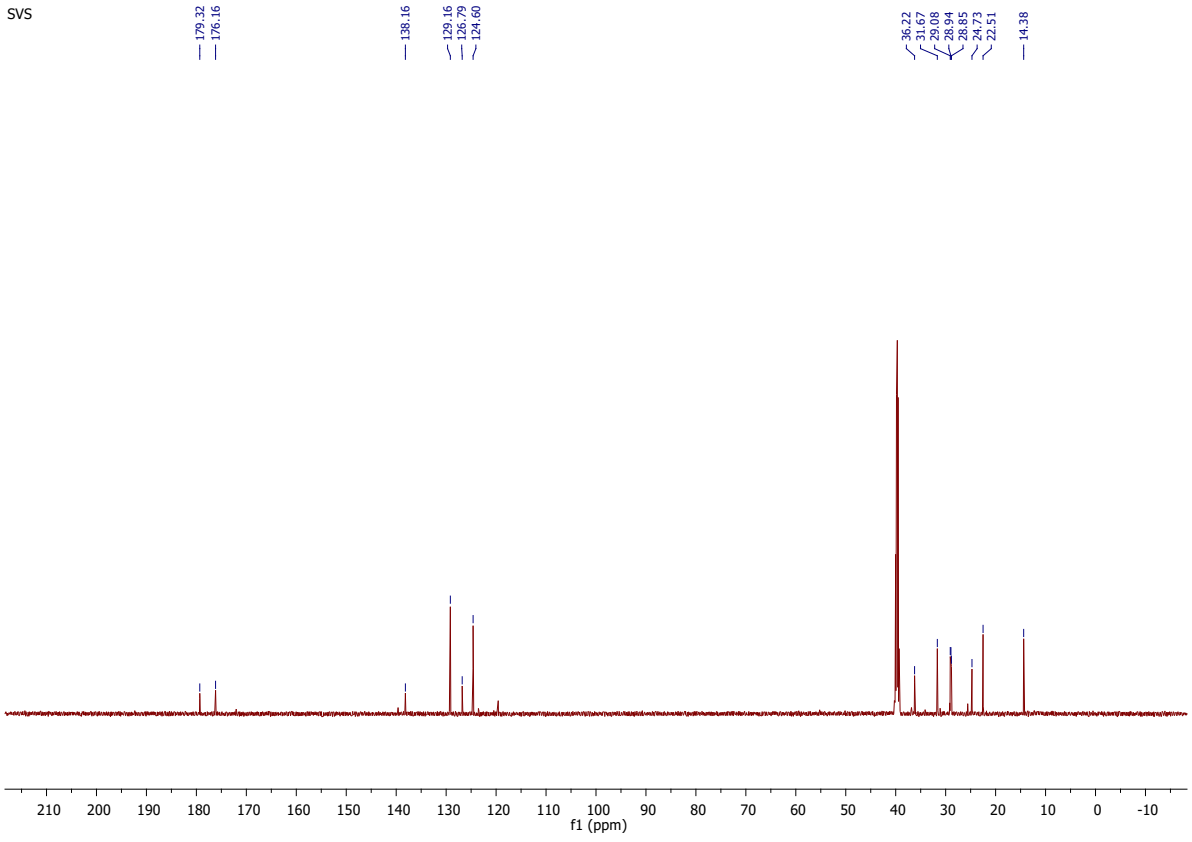

Figure S32. ^{13}C{^{1}H} NMR spectrum (100 MHz, DMSO-d_6) of L5.

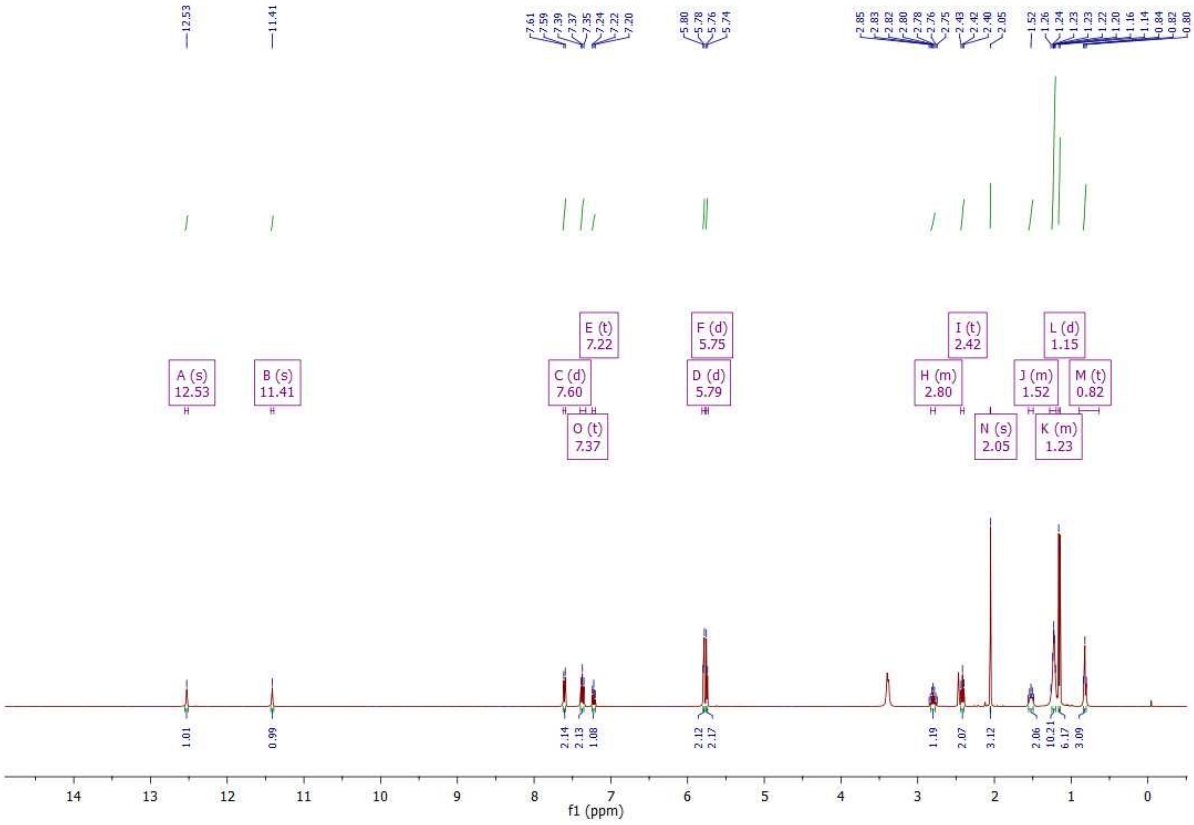

Figure S33. ^{1}H NMR spectrum (400 MHz, DMSO-d_6) of **P5**.

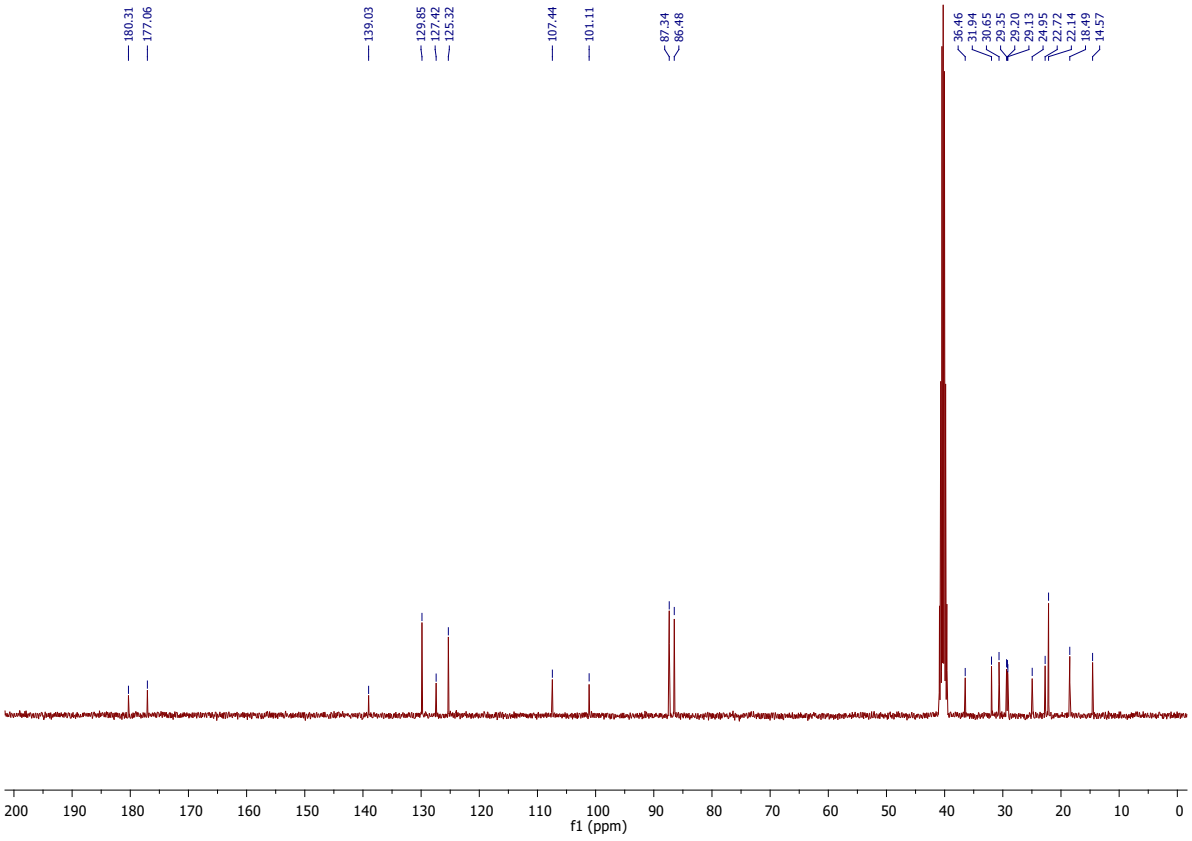

Figure S34. ^{13}C{^{1}H} NMR spectrum (100 MHz, DMSO-d_6) of **P5**.

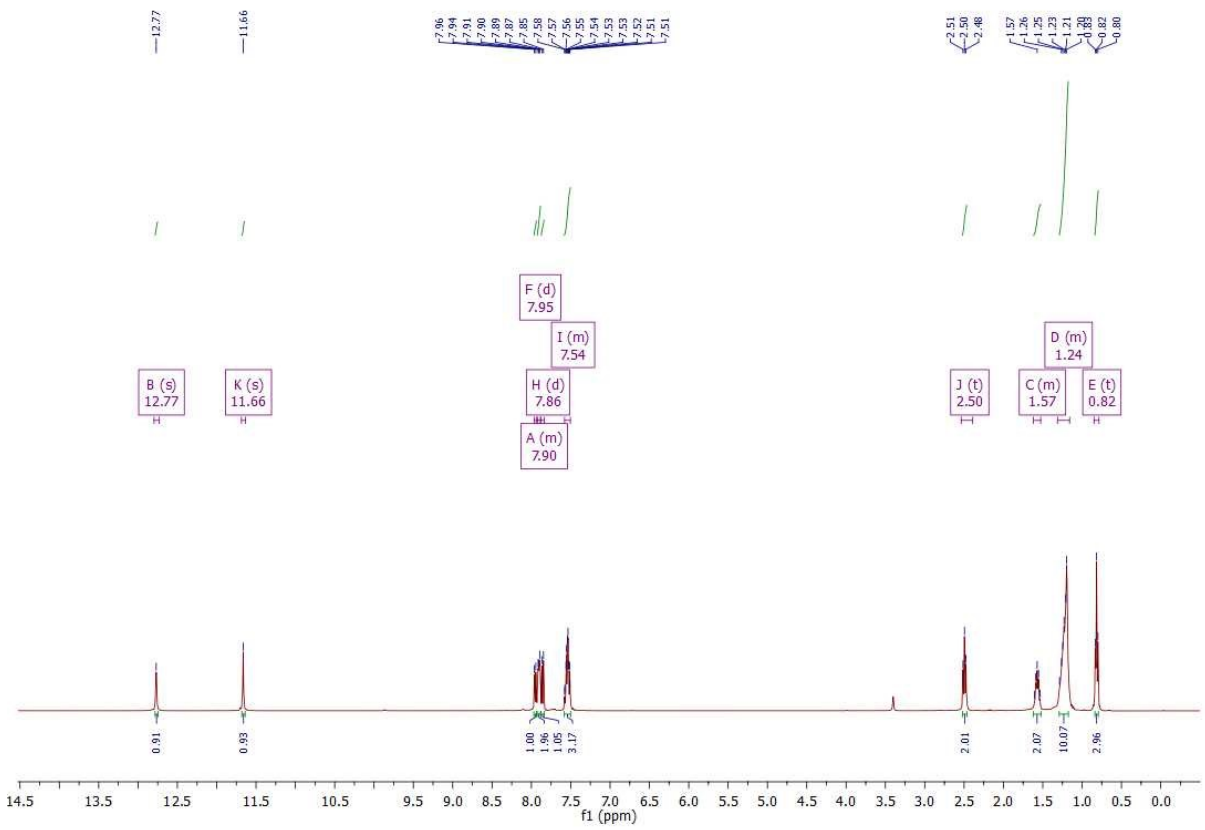

Figure S35. ^{1}H NMR spectrum (400 MHz, DMSO-d_6) of L6.

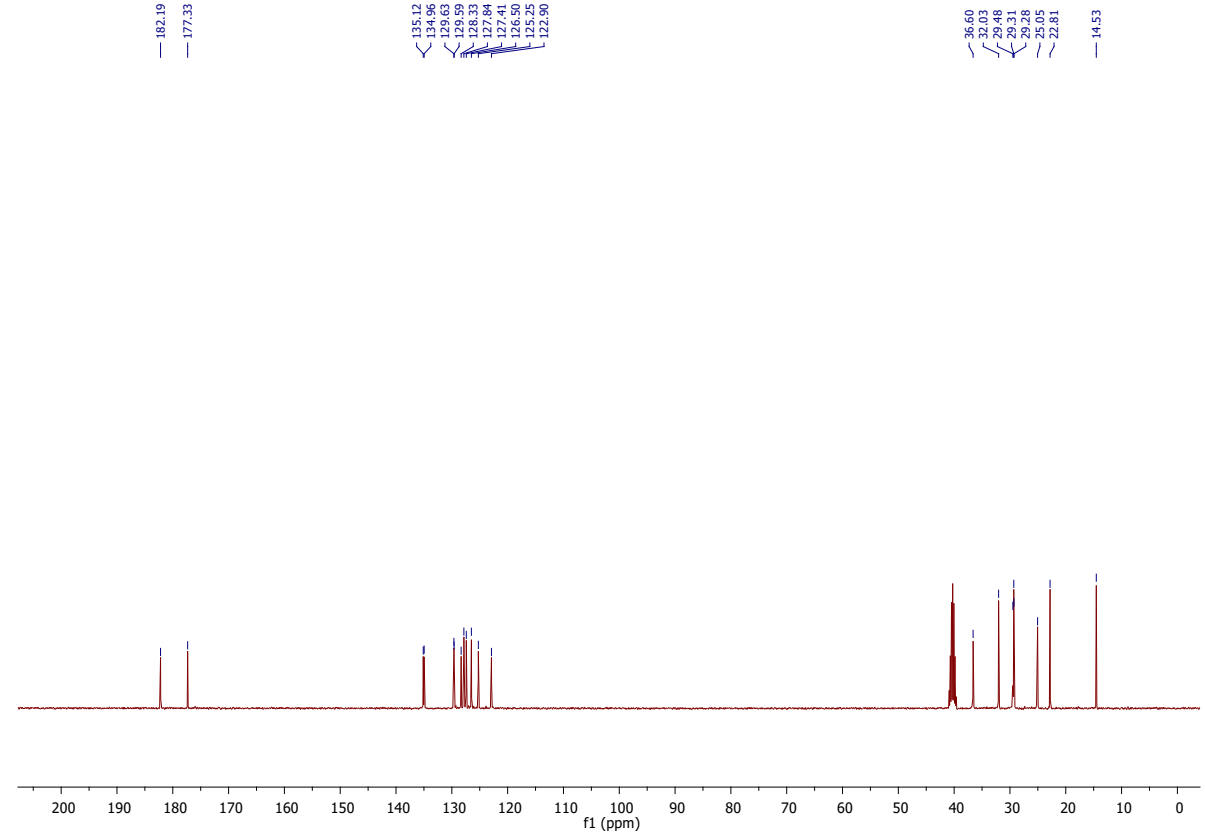

Figure S36. ^{13}C{^{1}H} NMR spectrum (100 MHz, DMSO-d_6) of L6.

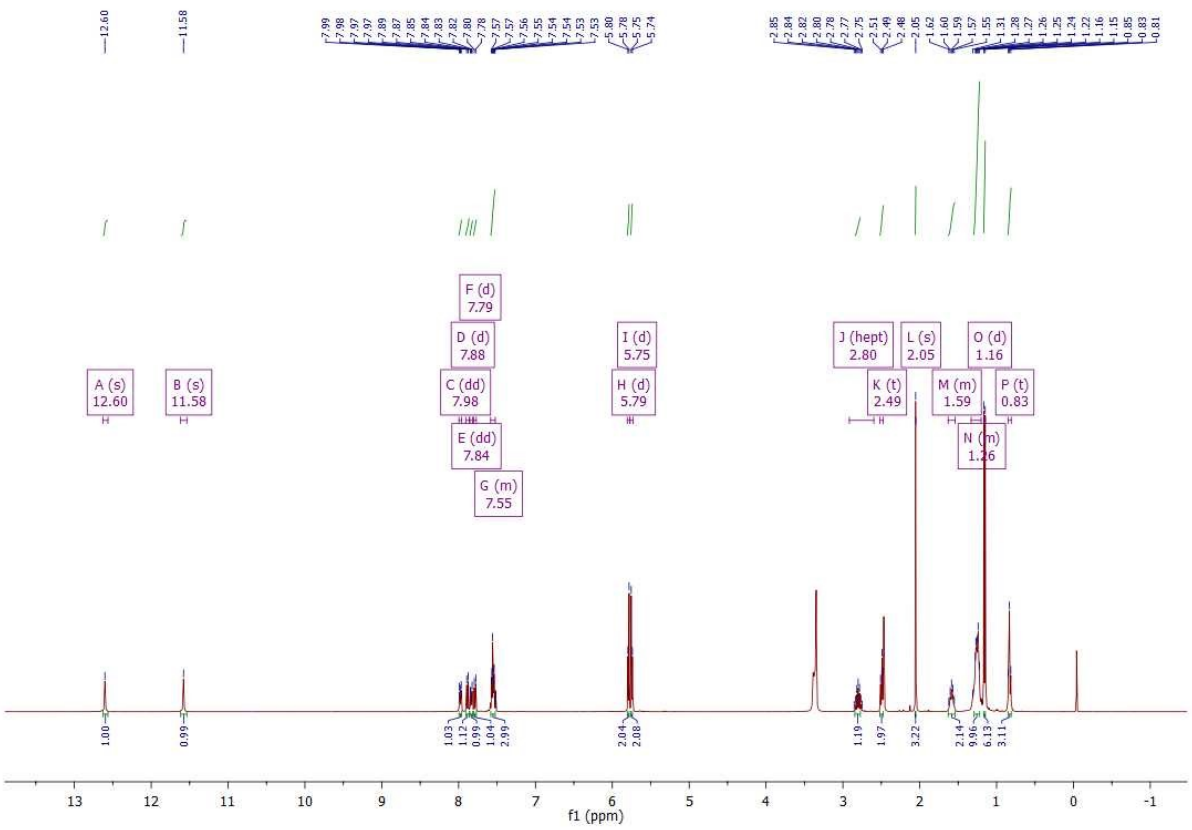

Figure S37. ^{1}H NMR spectrum (400 MHz, DMSO-d_6) of **P6**.

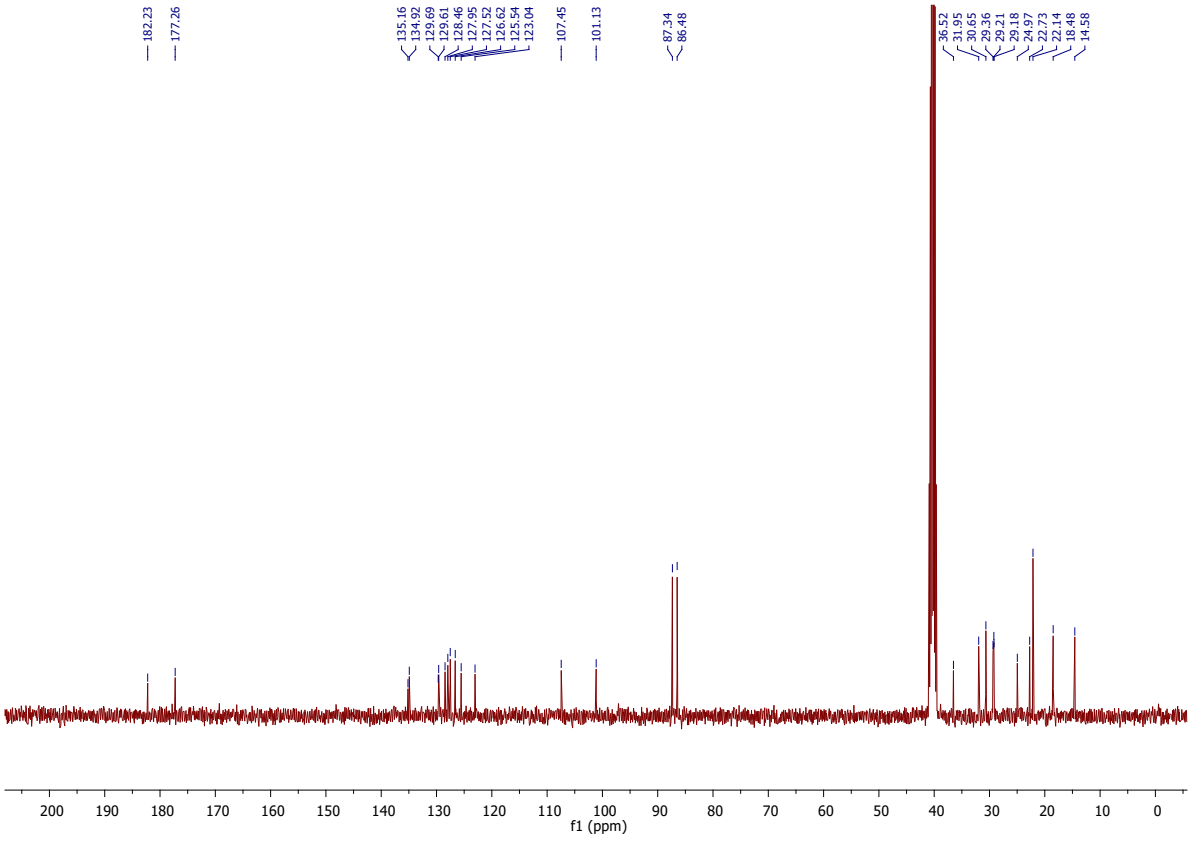

Figure S38. ^{13}C{^{1}H} NMR spectrum (100 MHz, DMSO-d_6) of **P6**.

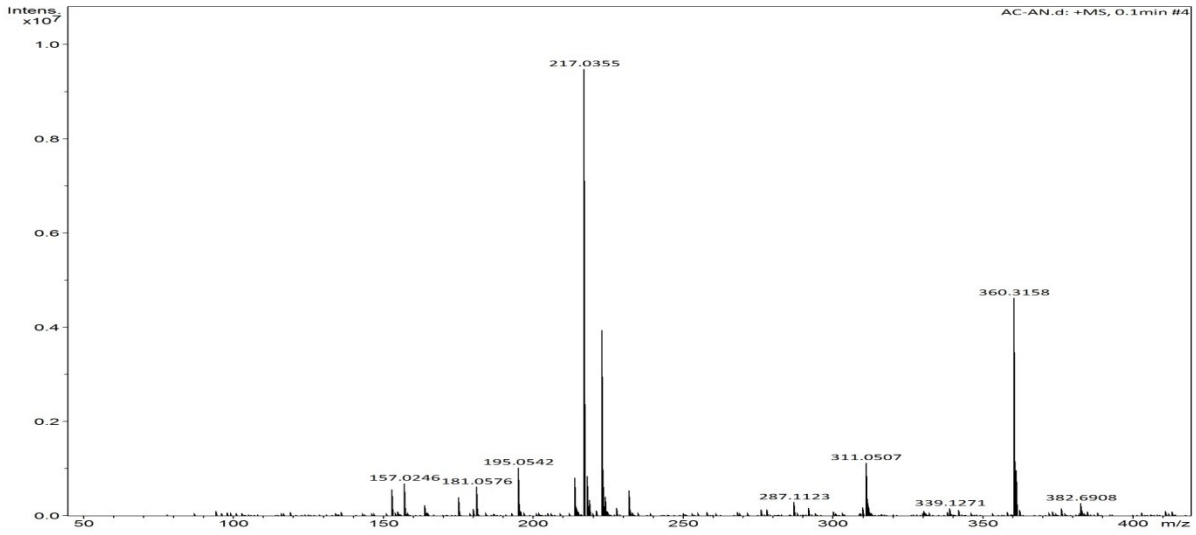

Figure S39. Mass spectrum of L1.

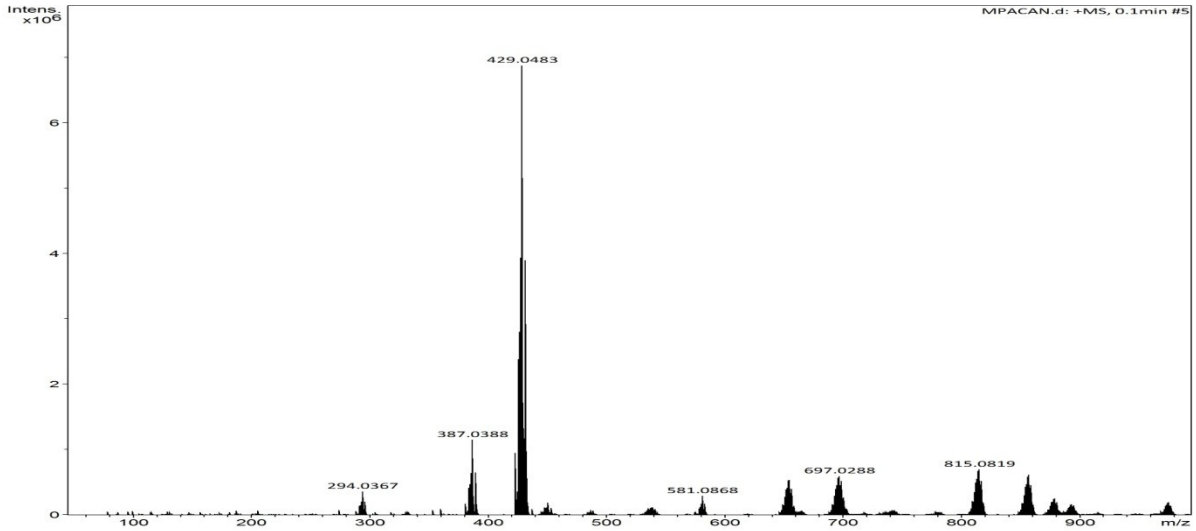

Figure S40. Mass spectrum of **P1**.

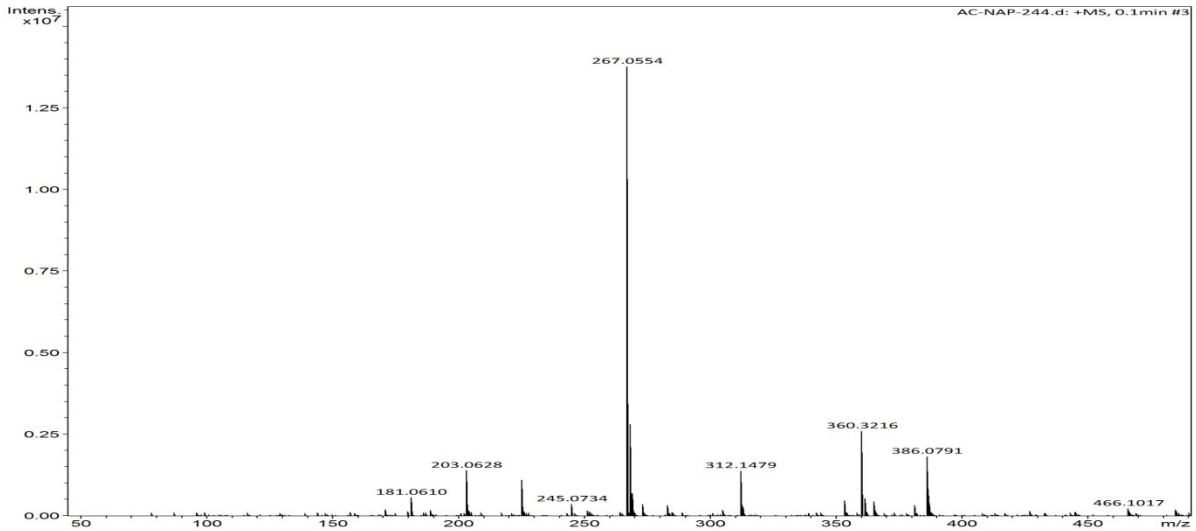

Figure S41. Mass spectrum of L2.

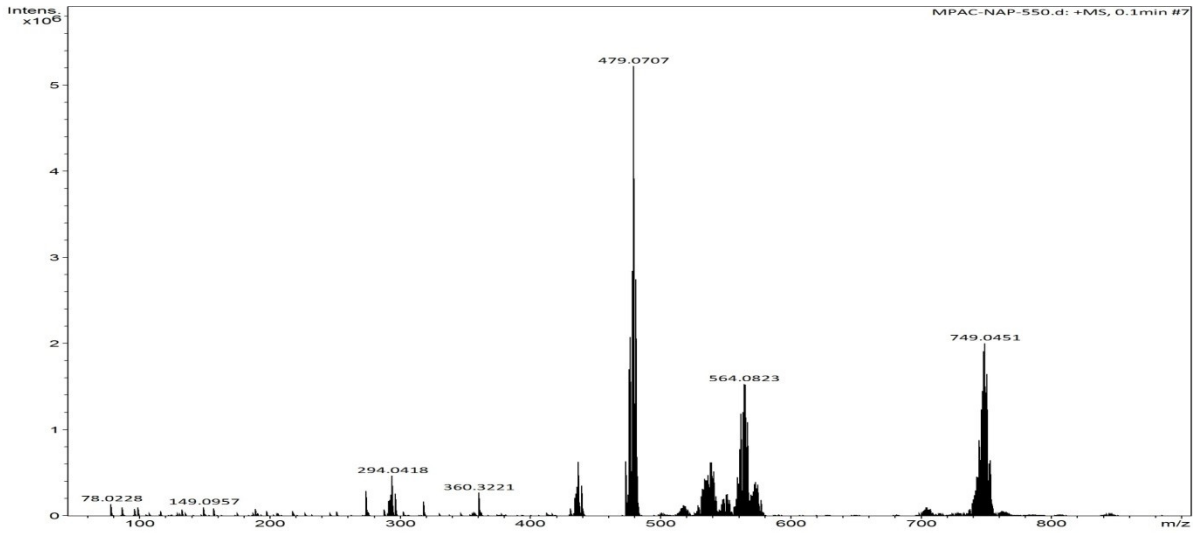

Figure S42. Mass spectrum of **P2**.

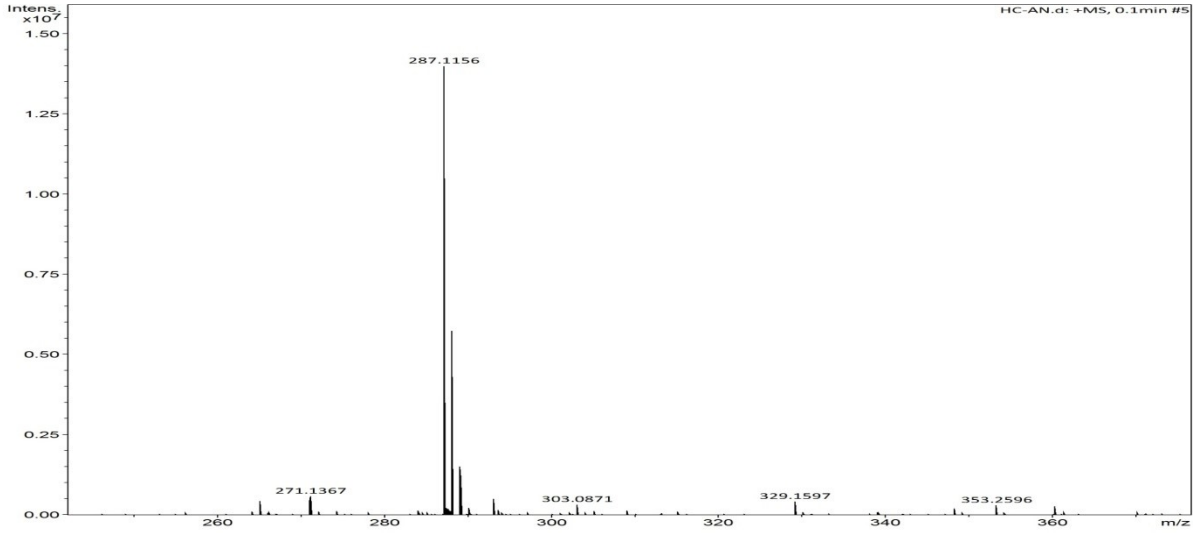

Figure S43. Mass spectrum of L3.

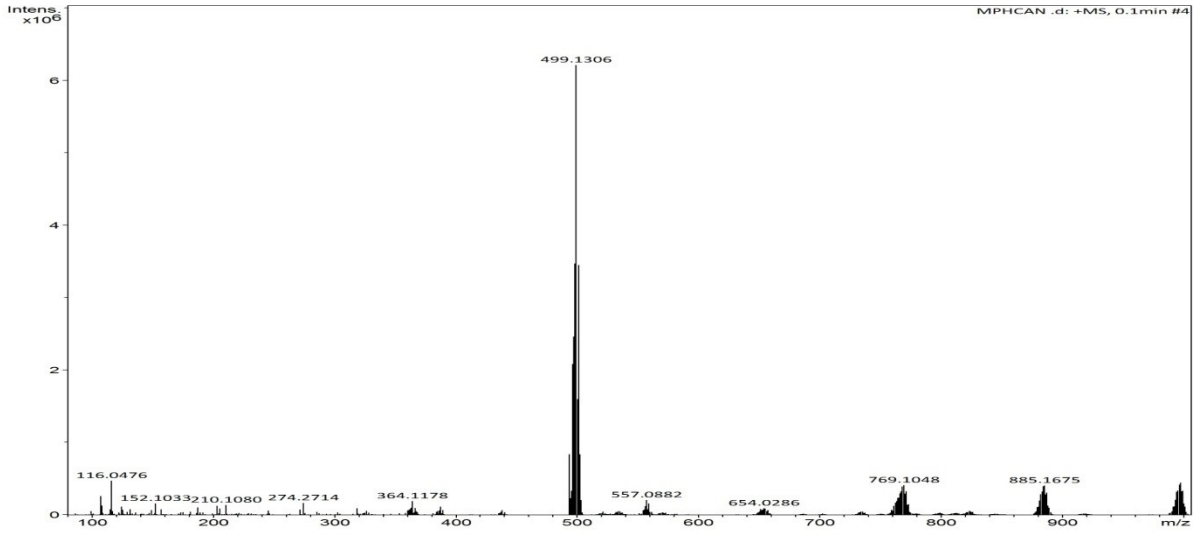

Figure S44. Mass spectrum of **P3**.

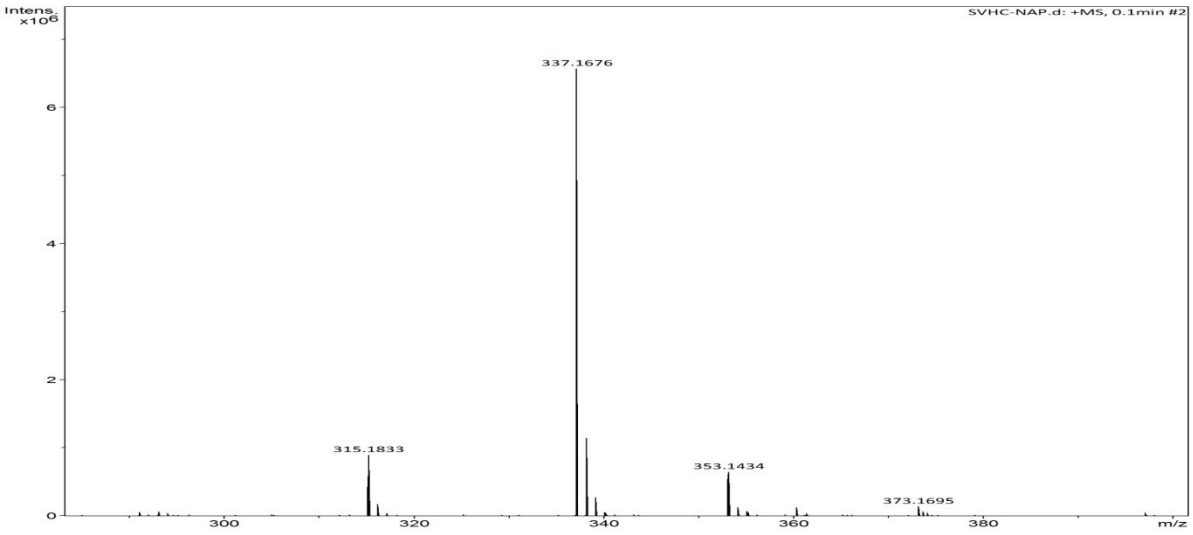

Figure S45. Mass spectrum of L4.

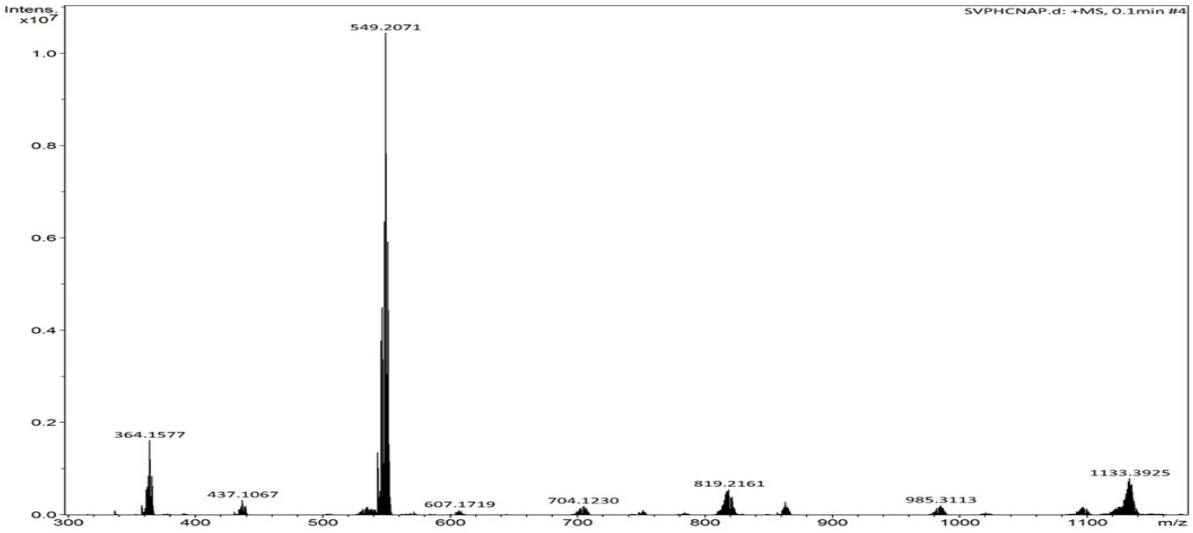

Figure S46. Mass spectrum of **P4**.

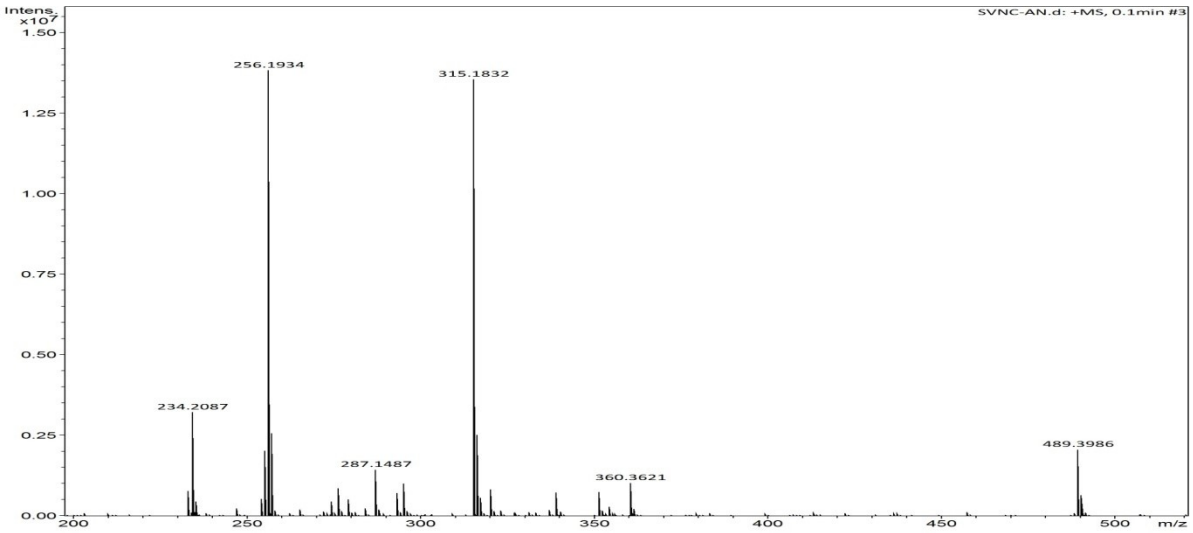

Figure S47. Mass spectrum of L5.

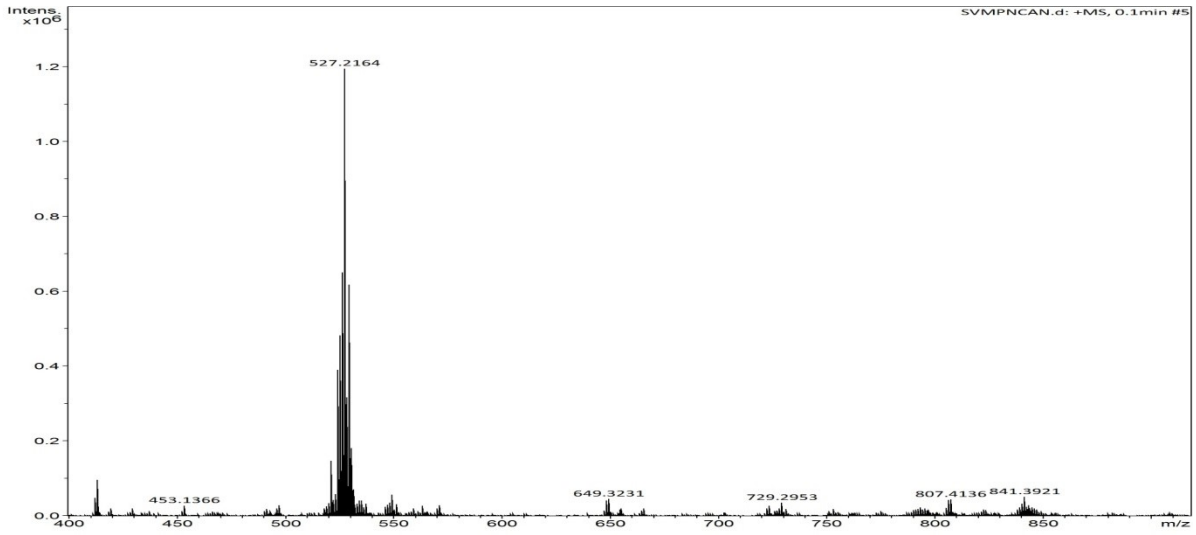

Figure S48. Mass spectrum of **P5**.

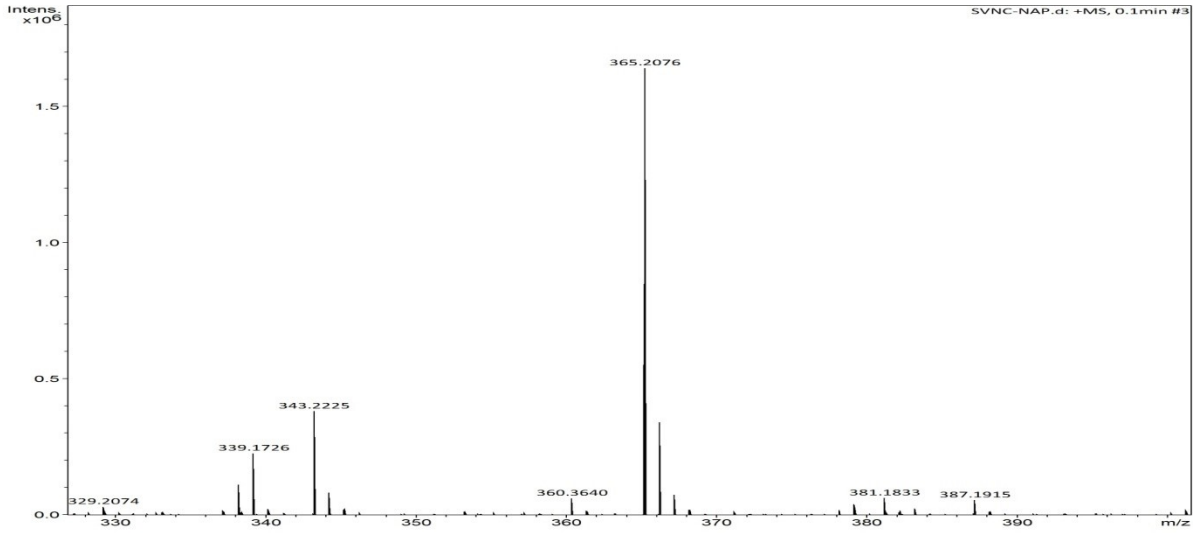

Figure S49. Mass spectrum of L6.

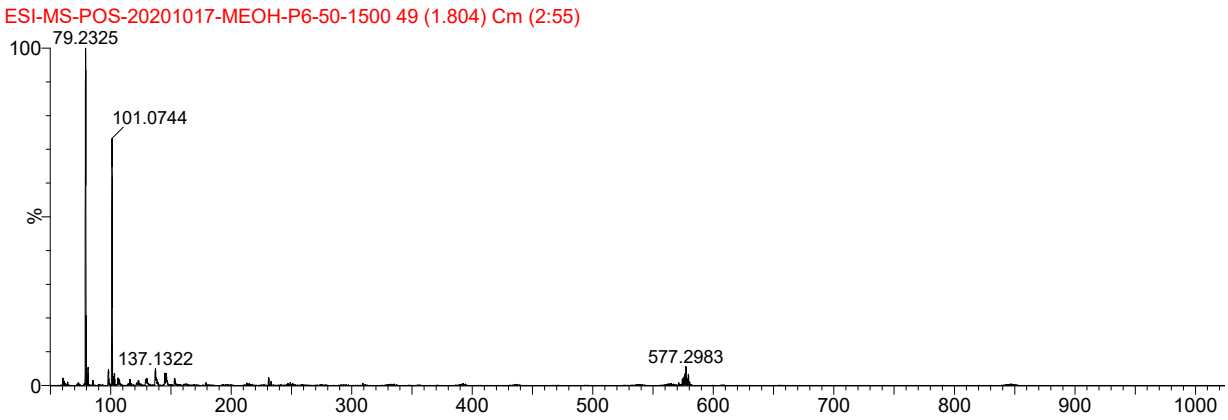

Figure S50. Mass spectrum of **P6**.

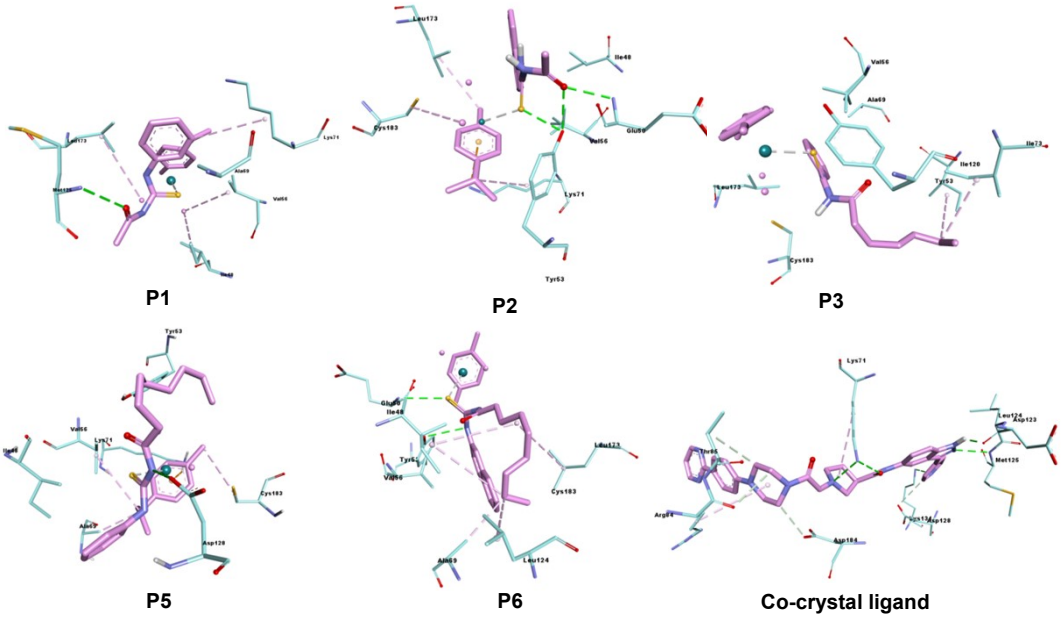
P1
P2
P3
P5
P6
Co-crystal ligand

(a)

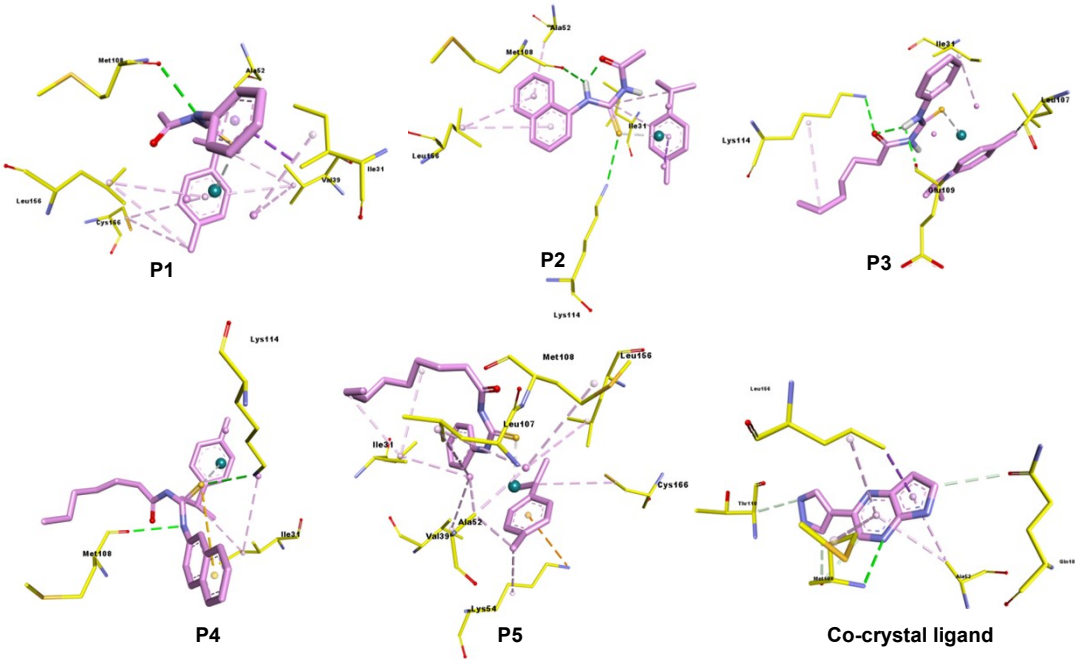
P1
P2
P3
P4
P5
Co-crystal ligand

(b)

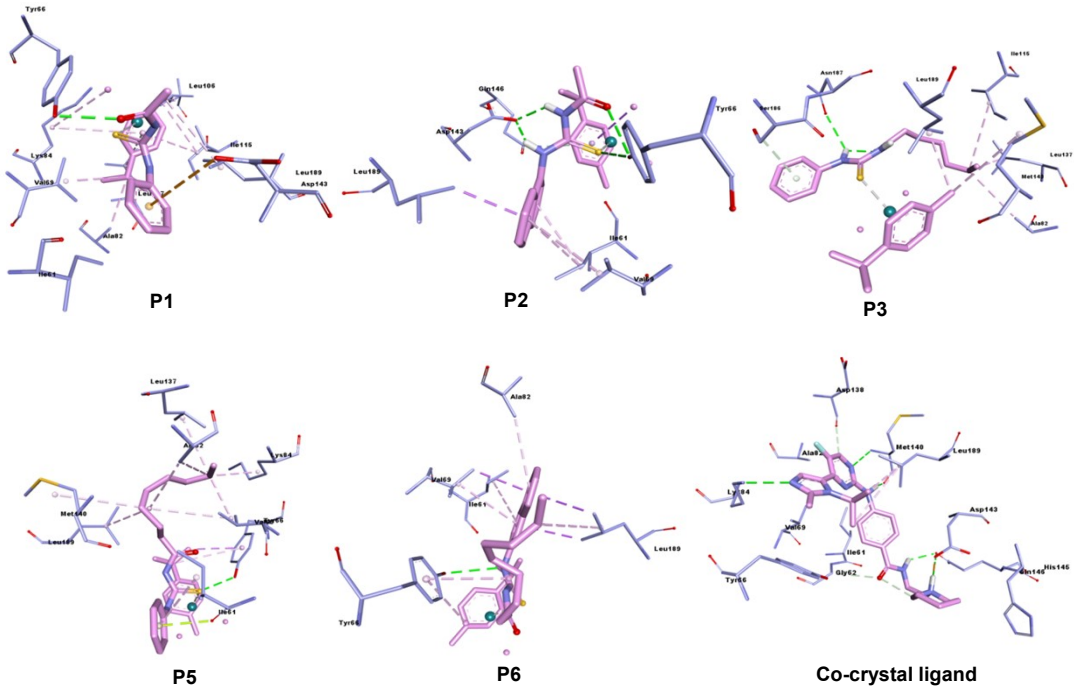
P1
P2
P3
P5
P6
Co-crystal ligand

(c)

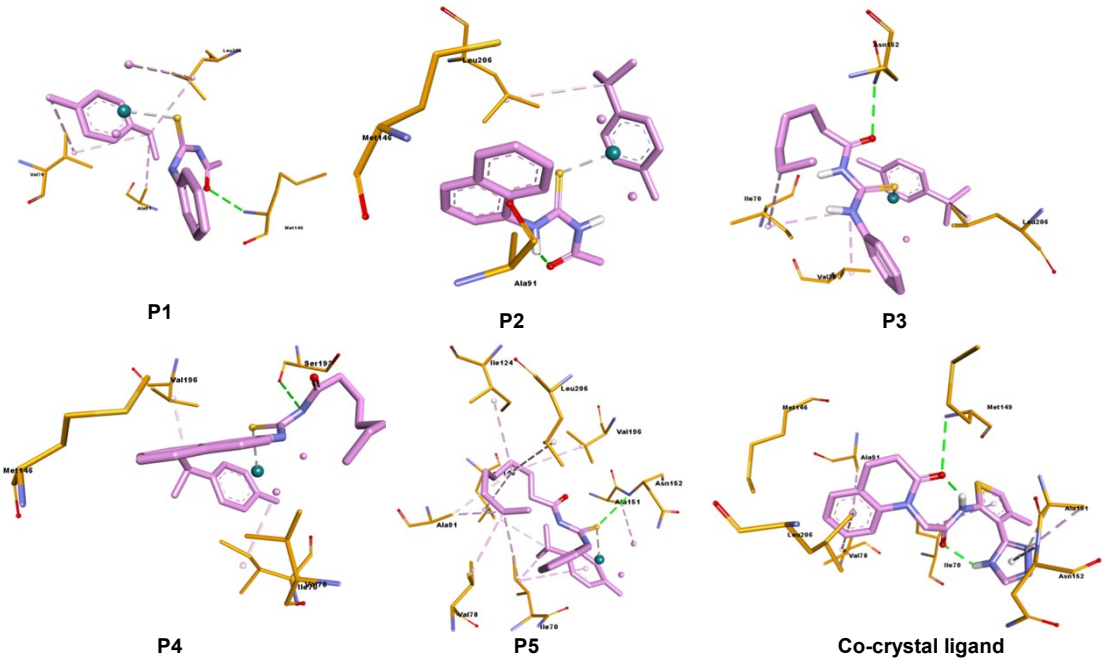
P1
P2
P3
P4
P5
Co-crystal ligand

(d)

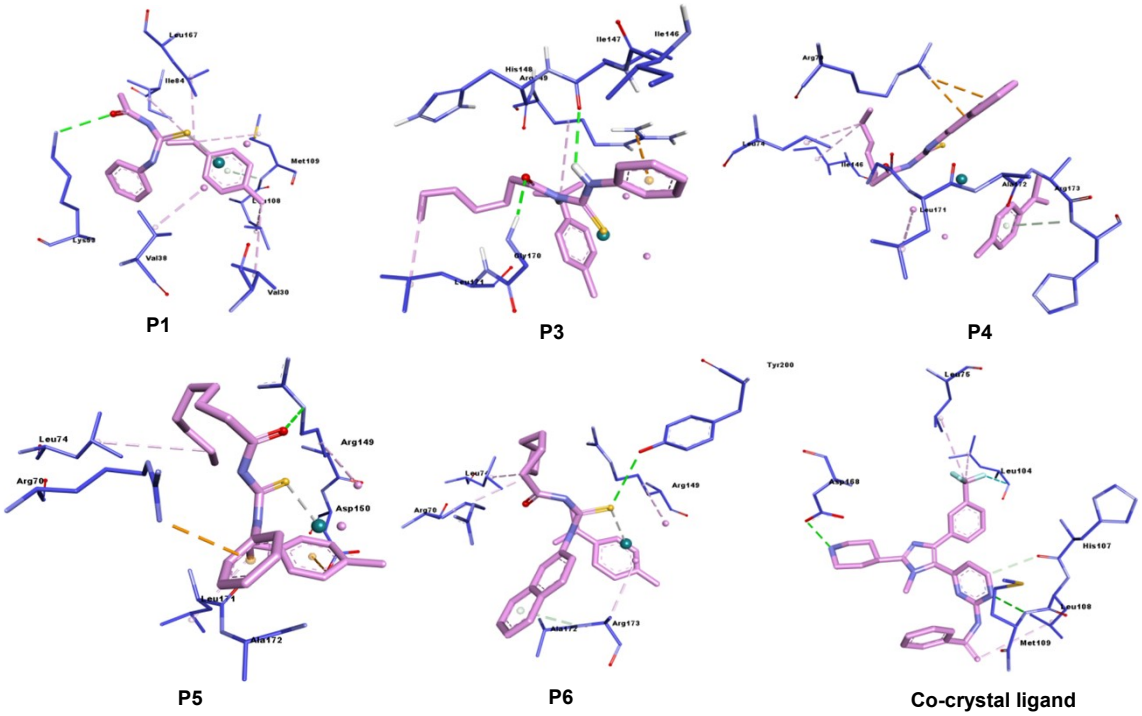

(e)

Figure S51. Interactions of **P1**-**P6** and the corresponding co-crystal ligand at the active site of (a) ERK1, (b) ERK2, (c) ERK5, (d) JNK and (e) p38 of MAPK pathway.

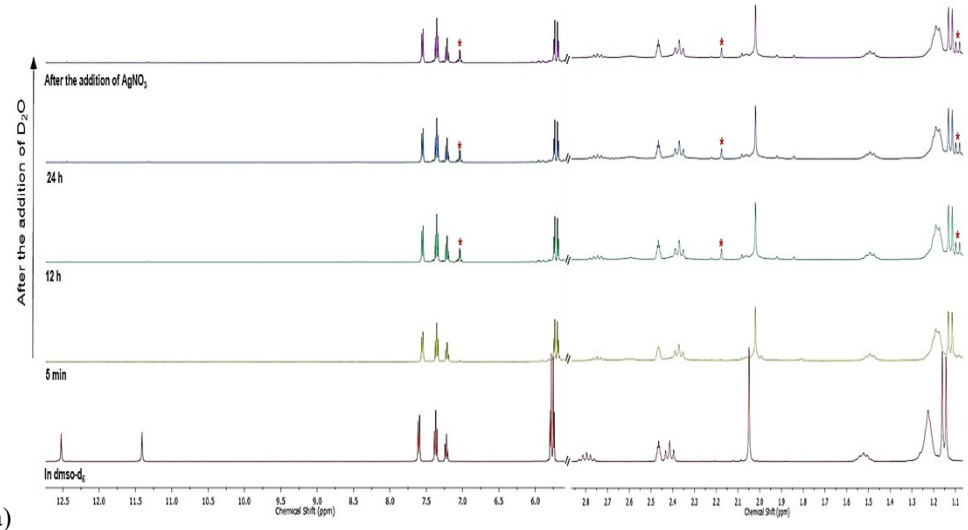

(a)

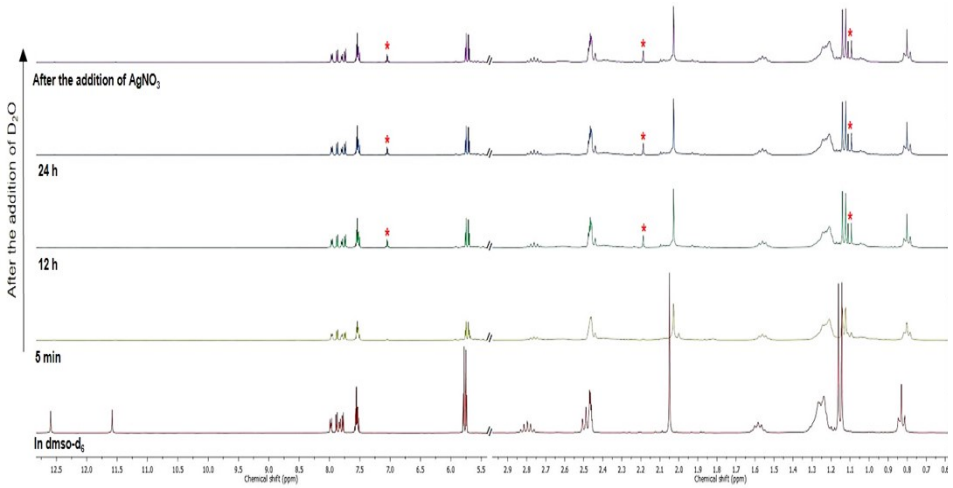

(b)

Figure S52. Time-dependent ^{1}H NMR spectra in DMSO(d_6)-D_2O (6:4) mixture of (a) **P5** and (b) **P6** over a period of 24 h, and after the addition of $AgNO_3$.

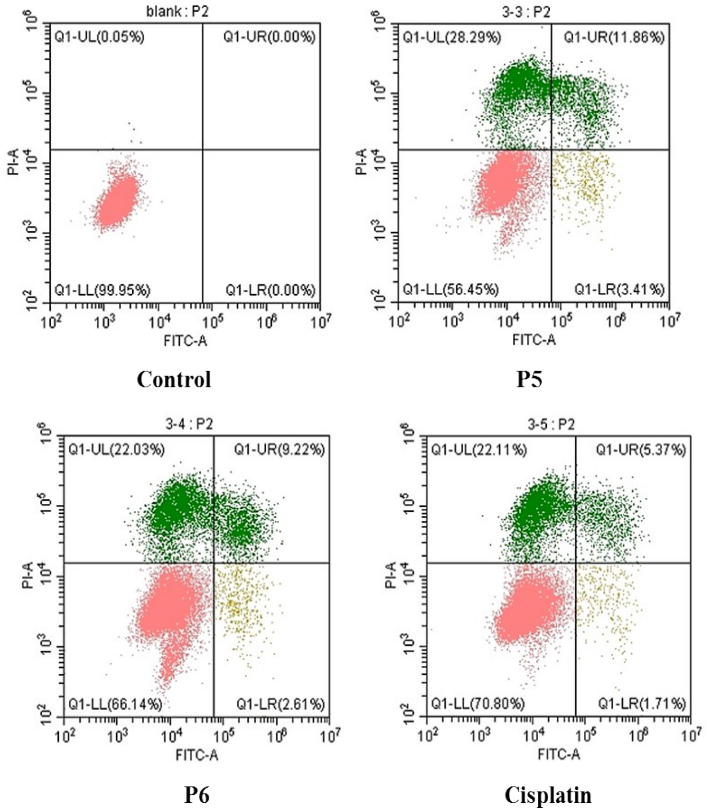

Figure S53. Alexa Fluor 488 Annexin V/propidium iodide (PI) double-staining assay of the selected complexes and cisplatin.

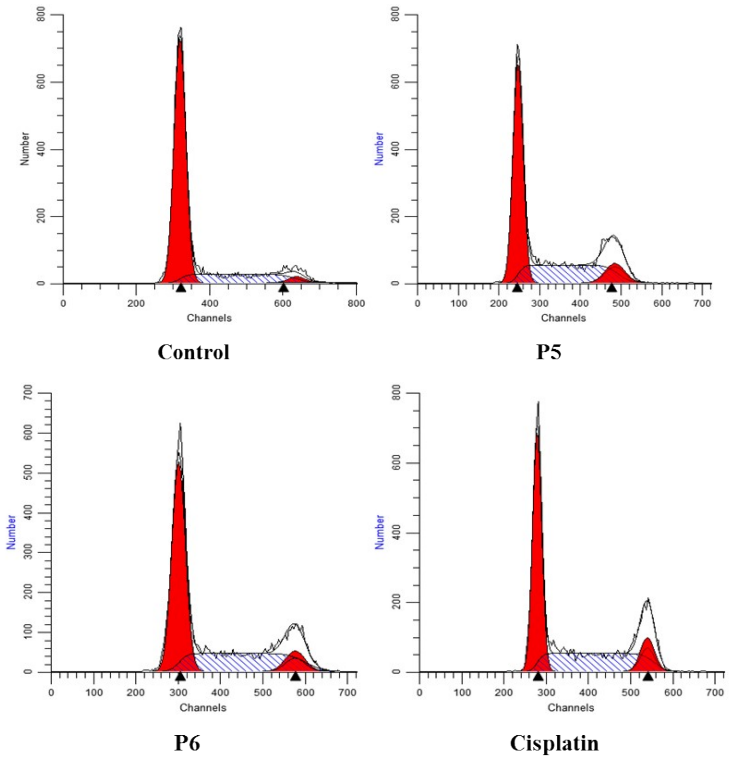

Figure S54. Cell cycle arrest of the selected complexes and cisplatin.

Table S1. Crystal data of L1, L3 and L5

	L1	L3	L5
Empirical formula	$C_9H_{10}N_2OS$	$C_{14}H_{20}N_2OS$	$C_{16}H_{24}N_2OS$
Formula weight	194.25	264.38	292.43
Temperature (K)	110.0	110.0	300.0
Wavelength (Å)	0.71073	0.71073	0.71073
Crystal system	Monoclinic	Triclinic	Monoclinic
Space group	P_12_1/c_1	*P*-1	*C*2/*c*
Unit cell dimensions			
a (Å)	9.9321(6)	9.5041(11)	34.4780(13)
b (Å)	22.3757(14)	10.2883(11)	5.2020(2)
c (Å)	8.8529(6)	15.1931(17)	18.8610(9)
α (°)	90	96.577(4)	90
β (°)	111.405(2)	99.785(4)	91.9433(18)
γ (°)	90	96.172(4)	90
Volume ($Å^3$)	1831.7(2)	1442.1(3)	3380.9(2)
Z	8	4	8
Density (calculated)	1.409	1.218	1.149

Mg/m^3			
Absorption coefficient (mm^{-1})	0.312	0.216	0.190
F(000)	816	568	1264
Crystal size (mm^3)	0.556 × 0.423 × 0.04	0.241 × 0.153 × 0.124	0.428 × 0.218 × 0.204
Theta range for data collection (°)	2.202 to 25.087	2.193 to 22.500	2.161 to 23.227
Index ranges	−11<=h<=11, −26<=k<=26, −10<=l<=10	−10<=h<=10, −11<=k<=10, −16<=l<=16	−38<=h<=38, −5<=k<=5, −20<=l<=14
Reflections collected	31733	9748	10181
Independent reflections [R(int)]	3271 [R(int) = 0.0920]	3710 [R(int) = 0.0467]	2410 [R(int) = 0.0312]
Absorption Correction	Semi-empirical from equivalents	Semi-empirical from equivalents	Semi-empirical from equivalents
Max. and min. transmission	0.6944 and 0.5437	0.7453 and 0.5685	0.7449 and 0.6611
Refinement method	Full-matrix least-squares on F^2	Full-matrix least-squares on F^2	Full-matrix least-squares on F^2
Data / restraints / parameters	3271 / 0 / 238	3710 / 334 / 393	2410 / 0 / 182
Goodness-of-fit on F^2	1.095	1.142	1.040
Final R indices [I>2sigma(*I*)]	R1 = 0.0457, wR2 = 0.0766	R1 = 0.0770, wR2 = 0.1586	R1 = 0.0349, wR2 = 0.0813
R indices (all data)	R1 = 0.0682, wR2 = 0.0839	R1 = 0.0939, wR2 = 0.1719	R1 = 0.0488, wR2 = 0.0899
Largest diff. peak and hole (e. $Å^{-3}$)	0.303 and −0.303	1.172 and −0.641	0.101 and −0.132

Table S2. Crystal data of **P2-P6**

	P2	P3	P4	P5	P6
Empirical formula	$C_{23}H_{26}Cl_2N_2ORuS$	$C_{24}H_{34}Cl_2N_2ORuS$	$C_{28}H_{36}Cl_2N_2ORuS$	$C_{26}H_{38}Cl_2N_2ORuS$	$C_{30}H_{40}Cl_2N_2ORuS$
Formula weight	550.49	570.56	620.62	598.61	648.67
Temperature (K)	110.0	110.0	110.0	110.0	110.0
Wavelength (Å)	0.71073	0.71073	0.71073	0.71073	0.71073
Crystal system	Monoclinic	Triclinic	Triclinic	Monoclinic	Triclinic
Space group	$P2_1/c$	P-1	P-1	$C2/c$	P-1
Unit cell dimensions					
a (Å)	9.1825(4)	9.3887(14)	10.3251(3)	17.5533(13)	10.4538(10)
b (Å)	12.6851(5)	10.7387(15)	14.2609(4)	13.3945(13)	16.6161(15)
c (Å)	19.9700(8)	13.0579(19)	20.2233(6)	24.754(2)	18.7518(17)
α (°)	90	106.287(4)	72.4080(10)	90	112.455(3)
β (°)	92.235(2)	94.363(5)	75.7970(10)	109.562(5)	95.919(3)
γ (°)	90	100.568(4)	85.5710(10)	90	91.536(3)
Volume (Å^3)	2324.35(17)	1230.9(3)	2751.74(14)	5484.1(8)	2986.4(5)
Z	4	2	4	8	4
Density (calculated) Mg/m^3	1.573	1.539	1.498	1.450	1.443
Absorption coefficient (mm^{-1})	1.012	0.958	0.864	0.864	0.800
F(000)	1120	588	1280	2480	1344
Crystal size (mm^3)	0.243 × 0.176 × 0.1490.243	0.469 × 0.287 × 0.154	0.561 × 0.542 × 0.278	0.41 × 0.405 × 0.107	0.325 × 0.221 × 0.153
Theta range for data collection (°)	2.220 to 23.907	2.188 to 24.998	2.035 to 30.543	2.463 to 27.610	2.095 to 27.500
Index ranges	−10<=h<=10, −14<=k<=14, −22<=l<=22	−11<=h<=11, −12<=k<=12, −15<=l<=15	−14<=h<=14, −20<=k<=20, −28<=l<=28	−22<=h<=22, −17<=k<=17, −32<=l<=32	−13<=h<=13, −21<=k<=21, −24<=l<=24
Reflections collected	22497	18148	137278	83206	223947

Independent reflections [R(int)]	3494 [R(int) = 0.0319]	4308 [R(int) = 0.0624]	16752 [R(int) = 0.0309]	6343 [R(int) = 0.0637]	13730 [R(int) = 0.0399]
Absorption correction	Semi-empirical from equivalents	Semi-empirical from equivalents	Semi-empirical from equivalents	Semi-empirical from equivalents	Semi-empirical from equivalents
Max. and min. transmission	0.4279 and 0.3531	0.3215 and 0.2160	0.3368 and 0.2653	0.4305 and 0.3082	0.4353 and 0.3959
Refinement Method	Full-matrix least-squares on F^2	Full-matrix least-squares on F^2	Full-matrix least-squares on F^2	Full-matrix least-squares on F^2	Full-matrix least-squares on F^2
Data / restraints / parameters	3494 / 0 / 275	4308 / 72 / 278	16752 / 0 / 639	6343 / 538 / 370	13730 / 393 / 724
Goodness-of-fit on F^2	1.310	1.118	1.035	1.088	1.057
Final R indices [I>2sigma(*I*)]	R1 = 0.0493, wR2 = 0.0836	R1 = 0.0534, wR2 = 0.1219	R1 = 0.0244, wR2 = 0.0634	R1 = 0.0318, wR2 = 0.0761	R1 = 0.0302, wR2 = 0.0698
R indices (all data)	R1 = 0.0565, wR2 = 0.0882	R1 = 0.0596, wR2 = 0.1285	R1 = 0.0300, wR2 = 0.0656	R1 = 0.0362, wR2 = 0.0790	R1 = 0.0348, wR2 = 0.0746
Largest diff. peak and hole (e. Å^{-3})	0.967 and –0.610	0.994 and –1.749	1.145 and –0.632	1.111 and –0.909	1.186 and –0.712

Table S3. Selected bond distances of **P2**-**P6**

	$C_{10}H_6$ as N-terminal substituent			C_6H_5 as N-terminal substituent	
	P2	**P4**	**P6**	**P3**	**P5**
Ru–Cl_1	2.430	2.461	2.448	2.409	2.421
Ru–Cl_2	2.425	2.436	2.418	2.446	2.441
Ru–$Cl_{(average)}$	2.428	2.449	2.433	2.428	2.431
Ru–S	2.434	2.413	2.416	2.414	2.399
Ru–C_1	2.159	2.218	2.162	2.162	2.171
Ru–C_2	2.163	2.168	2.178	2.178	2.173
Ru–C_3	2.176	2.194	2.291	2.181	2.176

Ru–C_4	2.187	2.219	2.201	2.196	2.185
Ru–C_5	2.193	2.172	2.202	2.218	2.185
Ru–C_6	2.206	2.181	2.212	2.233	2.211
Ru–$C_{(average)}$	2.180	2.192	2.191	2.194	2.18
C=S	1.702	1.700	1.698	1.699	1.703
C=O	1.216	1.219	1.216	1.210	1.214
C(alkyl)–CO	1.496	1.507	1.510	1.503	1.515
SC–NH(Ar)	1.327	1.325	1.332	1.329	1.321
SC–NH(CO)	1.363	1.367	1.369	1.369	1.369
HN–Ar	1.451	1.432	1.426	1.427	1.432
NH–CO	1.371	1.381	1.382	1.382	1.367

Table S4. ADME properties of the ligands and commercially available drugs

	L1	L2	L3	L4	L5	L6	**Irinotecan**	**Etoposide**
Physicochemical Properties								
Molecular weight (g mol^{-1})	194.25	244.31	264.39	314.45	292.44	342.50	586.68	588.56
Heavy atoms	13	17	18	22	20	24	43	42
Aromatic heavy atoms	6	10	6	10	6	10	16	12
Fraction Csp^3	0.11	0.08	0.43	0.33	0.50	0.40	0.52	0.55
Rotatable bonds	4	4	9	9	11	11	6	5
H-bond acceptors	1	1	1	1	1	1	8	13
H-bond donors	2	2	2	2	2	2	1	3
Molar refractivity	56.15	73.66	80.19	97.70	89.90	107.31	169.63	139.11
TPSA [$Å^2$]	73.22	73.22	73.22	73.22	73.22	73.22	114.20	160.83
Consensus log $P_{o/w}$	1.73	2.48	3.31	4.13	4.08	4.77	3.73	1.13
Pharmacokinetics								
GI absorption	High	High	High	High	High	High	High	Low
BBB permeant	No	Yes	Yes	Yes	Yes	No	No	No
Pgp substrate	No	No	No	No	No	No	Yes	Yes
CYP1A2 inhibitor	Yes	Yes	Yes	Yes	Yes	Yes	No	No
CYP2C19 inhibitor	No	Yes	Yes	Yes	Yes	Yes	No	No
CYP2C9 inhibitor	No	No	Yes	Yes	Yes	Yes	Yes	No
CYP2D6 inhibitor	No	No	No	Yes	No	Yes	Yes	Yes
CYP3A4 inhibitor	No	No	No	Yes	Yes	Yes	Yes	No

Log K_p[cm/s]	-5.92	-6.10	-4.85	-4.78	-4.26	-4.19	-7.22	-9.46
Drug-likeness								
Lipinski	Yes	Yes	Yes	Yes	Yes	Yes	Yes	No
Ghose	Yes	Yes	Yes	Yes	Yes	Yes	No	No
Veber	Yes	Yes	Yes	Yes	No	No	Yes	No
Egan	Yes	Yes	Yes	Yes	Yes	Yes	Yes	No
Muegge	No	Yes	Yes	Yes	No	No	Yes	No
Bioavailablity score	0.55	0.55	0.55	0.55	0.55	0.55	0.55	0.17
Medicinal chemistry								
PAINS	0	0	0	0	0	0	0	0
Lead-likeness	No	No	No	No	No	No	No	No
Synth. accessibility	1.67	1.89	2.30	2.53	2.52	2.75	5.59	6.27

Table S5. Apoptosis ratio of the complexes

Sample	Apoptosis ratio
Control	0
P5	43.56
P6	33.83
Cisplatin	29.19

Table S6. Cell cycle analysis of the complexes

Sample	G0/G1 phase	S phase	G2/M phase
Control	83.35	15.56	1.09
P5	54.51	41.15	4.32
P6	57.32	38.57	4.11
Cisplatin	58.84	36.16	7.99

References

[1] S. Swaminathan, J. Haribabu, K.N. Kumar, N. Maroli, N. Balakrishnan, N. Bhuvanesh, K. Krishna, P. Kolandaivel, R. Karvembu, Tunable anticancer activity of furoylthiourea-based Ru(II)-arene complexes and their mechanism of action, Chem. –Eur. J. 2021, **27**, 7418–7433. https://doi.org/10.1002/chem.202004954.

[2] APEX2 "Program for Data Collection and Integration on Area Detectors", Bruker AXS Inc., 5465 East Cheryl Parkway, Madison, WI 53711-5373 USA.

[3] G. M. Sheldrick, A short history of SHELX, *Acta Cryst*. 2008, **A64**,112-122.

[4] G. M. Sheldrick, SHELXT - Integrated space-group and crystal-structure determination, *Acta Cryst*. 2015, **A71**, 3-8.

[5] G. M. Sheldrick, Crystal structure refinement with SHELXL, *Acta Cryst*. 2015, **C71**, 3-8.

[6] O. V. Dolomanov, L. J. Bourhis, R. J. Gildea, J. A. K. Howard, H. Puschmann, OLEX2: a complete structure solution, refinement and analysis program. *J. Appl. Crystallogr*. 2009, **42**, 339-341.

[7] C.A. Lipinski, F. Lombardo, B.W. Dominy, P.J. Feeney, Experimental and computational approaches to estimate solubility and permeability in drug discovery and development settings, *Adv. Drug Deliv. Rev*. 1997, **23**, 3–25. https://doi.org/10.1016/S0169-409X(96)00423-1.

[8] J. Bojarska, M. Remko, M. Breza, I. D. Madura, K. Kaczmarek, J. Zabrocki, W.M. Wolf, A supramolecular approach to structure-based design with a focus on synthons hierarchy in ornithine-derived ligands: review, synthesis, experimental and in silico studies, *Molecules* 2020, **25**, 1135. https://doi.org/10.3390/molecules25051135.

[9] T. Liu, Y. Lin, X. Wen, R.N. Jorissen, M.K. Gilson, BindingDB: A web-accessible database of experimentally determined protein–ligand binding affinities, *Nucleic Acids Res*. 2007, **35**, D198–D201. https://doi.org/10.1093/nar/gkl999.

[10] G.M. Morris, R. Huey, W. Lindstrom, M.F. Sanner, R.K. Belew, D.S. Goodsell, A.J. Olson, AutoDock4 and AutoDockTools4: Automated docking with selective receptor flexibility, *J. Comput. Chem*. 2009, **30**, 2785–2791. https://doi.org/10.1002/jcc.21256.

[11] M.K. Mohamed Subarkhan, L. Ren, B. Xie, C. Chen, Y. Wang, H. Wang, Novel tetranuclear ruthenium(II) arene complexes showing potent cytotoxic and antimetastatic activity as well as low toxicity in vivo, *Eur. J. Med. Chem*. 2019, **179**, 246–256. https://doi.org/10.1016/j.ejmech.2019.06.061.

[12] K. Jeyalakshmi, J. Haribabu, N.S.P. Bhuvanesh, R. Karvembu, Half-sandwich $RuCl_2(\eta^6$-*p*-cymene) core complexes containing sulfur donor aroylthiourea ligands: DNA and protein binding, DNA cleavage and cytotoxic studies, *Dalton Trans*. 2016, **45**, 12518–12531. https://doi.org/10.1039/c6dt01167e.

[13] S. Swaminathan, J. Haribabu, N. Kumar Kalagatur, R. Konakanchi, N. Balakrishnan, N. Bhuvanesh, R. Karvembu, Synthesis and anticancer activity of $[RuCl_2(\eta^6$-arene)(aroylthiourea)] complexes—High

activity against the human neuroblastoma (IMR-32) cancer cell line, *ACS Omega*, 2019, **4**, 6245–6256. https://doi.org/10.1021/acsomega.9b00349.